A PARAMETRIC STUDY OF THE RADIANT ENERGY FLUX TO THE FUEL SURFACE DURING HYBRID COMBUSTION

CARL EUGENE BRUNTLETT

A PARAMETRIC STUDY OF THE RADIANT ENERGY FLUX TO THE FUEL SURFACE DURING HYBRID COMBUSTION

by

Carl Eugene Bruntlett
Lieutenant, United States Navy
B.S., Naval Academy, 1960

Submitted in partial fulfillment of the
requirements for the degree of

MASTER OF SCIENCE IN AERONAUTICAL ENGINEERING

from the

NAVAL POSTGRADUATE SCHOOL
December 1967

ABSTRACT

The heat transfer rate to the solid fuel surface during hybrid combustion has been considered as the primary rate limiting phenomenon in one theoretical analysis of the hybrid combustion process. One mode of heat transfer involved is the radiant energy flux to the fuel surface. Little data are available for direct measurement of this portion of the heat transfer. Experiments were conducted in which the radiant flux to the fuel surface was measured by utilizing thin-film thermometers as a heat sensing device. A limited amount of data was obtained for the radiant flux during combustion of the polystyrene-oxygen system. These data established a range of values for the radiant flux of 10-14 BTU/ft^{2}sec. Combustion chamber pressure was varied between 7 and 14 atmospheres. Values of oxidizer mass flux, 0.15 and 0.24 lbm/in^{2}sec, were used to obtain the data. The results appeared to verify the analytical formulation for fuel linear regression rate in terms of the physical coupling between the convective and radiative heat transfer rates to the fuel surface.

Thesis of Carl E. Bruntlett, titled "A Parametric Study of the Radiant Energy Flux to the Fuel Surface During Hybrid Combustion.

ERRATA SHEET

Page	Line	Change	To
2	16/17	analy-tical	analyt-ical
11	2	greatfully	gratefully
15	6/7	neg-lected	ne-glected
18	14/15	investiga-ted	investigat-ed
26	17	pace	Pace
27	1	1172BB provided	1172BB gage provided
83	Item 13, 2/3	phenom-enon	pheno-menon
83	Item 13, 10/11	esta-blished	estab-lished

TABLE OF CONTENTS

LIST OF TABLES

LIST OF ILLUSTRATIONS

TABLE OF SYMBOLS

Symbol	Definition
B	Mass Transfer Parameter
B_l	Thermodynamic Mass Transfer Parameter
c_s	Substrate Specific Heat
G	Total Mass Flux
G_o	Oxidizer Mass Flux
h_{eff}	Effective Heat of Gasification of Fuel
I_h	Heat Sensor Excitation Current
k_s	Substrate Thermal Conductivity
$\dot{m}_f$	Fuel Mass Burning Rate
$\dot{m}_o$	Oxygen Mass Flow Rate
n	Radiating Particle Density in Gas Stream
P_b	Combustion Chamber Pressure
P_o	Plenum Chamber Pressure
P_r	Prandtl Number
$\dot{Q}_c$	Convective Heat Transfer Rate
$\dot{Q}_g$	Radiative Heat Transfer Rate Measured by Heat Sensor
$\dot{Q}_r$	Radiative Heat Transfer Rate
R	Electrical Resistance
R_{ex}	Reynolds Number Based on Length
$\dot{r}$	Linear Regression Rate
$\dot{r}_c$	Calculated Linear Regression Rate $\dot{r}_c = \frac{\dot{m}_f}{\rho_f S}$
S	Burning Surface Area
T	Temperature
T_r	Effective Radiation Temperature of System

Symbol	Definition
t	Time
t_b	Burning Time
V	Voltage
x	Length
z	Optical Path Length
α	Empirical Constant
β	Empirical Constant
ϵ_w	Fuel Surface Emissivity
ζ	Integration Parameter
λ	Weight Fraction of Gas in Decomposed Fuel Grain at Equilibrium Wall Temperature
μ	Gas Viscosity
ρ_f	Fuel Density
ρ_s	Substrate Density
σ	Stephan-Bolzmann Constant
τ	Thickness

ACKNOWLEDGEMENTS

The author is indebted to the following gentlemen and greatfully acknowledges their contributions:

Dr. R. E. Reichenbach, Associate Professor of Aeronautics, Naval Postgraduate School, Monterey, California, for technical assistance in the conduct of this research effort.

Mr. T. B. Dunton whose experience and technical skill made construction of the heat sensing instrumentation possible.

Messrs. E. J. Smith, E. Michelson, and C. R. Gordon who assisted in installing the apparatus and conducting the experiments.

SECTION 1

INTRODUCTION

The hybrid rocket, which utilizes liquid oxidizer and solid fuel, has been studied for some time. This type of rocket motor has relatively simple thrust modulation and restart capabilities. The ability to predict solid fuel regression rates analytically would be valuable to the hybrid rocket propulsion system designer. Accurate prediction of regression rate as a function of system parameters requires an understanding of the combustion process. Research efforts in the hybrid field have included several theoretical analyses of the combustion system. Concurrently, various investigators developed methods of measuring regression rates during hybrid combustion processes. The hybrid combustion process has been modeled as a chemically reacting boundary layer with mass addition. The emphasis on the use of ablative material on re-entry vehicles spurred investigation of this type of boundary layer. A review of several different models of the hybrid combustion process is presented by Green.[1]

A boundary layer with a diffusion controlled combustion process occurring within it was one of the models proposed. Penner analyzed this model.[2] The adoption of the Burke-Schummann solution limited the validity of this analysis to laminar boundary layers.[1] Another of the models proposed was that of a turbulent boundary layer with a

diffusion controlled combustion process occurring within it. Marxman and Gilbert obtained an analytical solution for this model.[3] Marxman, et al., have examined this model in detail, and they have conducted experimental studies of the combustion processes.[4,5,22] The heat flux from the combustion zone to the fuel surface is considered the primary rate controlling factor. The model approximates the reaction zone as a thin sheet within the boundary layer, which causes a discontinuity in the boundary layer temperature gradient. Flame location within the boundary layer is dependent upon the local oxidizer-fuel ratio.[3] Figure 1 is a schematic representation of the model. The analysis of the model considers as parameters: pressure, oxidizer mass flux, flame temperature, and geometry of the burning surface. The regression rate can be expressed in terms of the heat transfer rates as

$$\dot{r} = \frac{\dot{Q}_c}{\rho_f h_{eff}} \left[\frac{\dot{Q}_r}{\dot{Q}_c} + e^{-\frac{\dot{Q}_r}{\dot{Q}_c}} \right]. \tag{1}$$

The convective heat transfer rate ($\dot{Q}_c$) can be expressed as

$$\dot{Q}_c = h_{eff} \left[0.036\, B^{0.23} P^{0.23\beta} G\, R_{ex}^{-0.2} \right], \tag{2}$$

while the radiative heat transfer rate ($\dot{Q}_r$) equals

$$\dot{Q}_r = \sigma \epsilon_w T_r^4 \left[1 - e^{\alpha n z} \right]. \tag{3}$$

In the previous relations h_{eff} is the effective heat of gasification of the fuel. For fuels which resemble a plastic, h_{eff} includes the heat required to raise the fuel to the surface temperature, the energy required for depolymerization, and the heat of gasification of the monomer. The radiant heat transfer rate will be small and can be neglected for fuel-oxidizer systems whose combustion products do not include a large number of solid particles.

Smoot and Price have developed the following expression for the regression rate using a turbulent boundary layer model.[6]

$$\dot{r} = 0.03 \left(\frac{G^{0.8}}{\rho_f \lambda}\right)\left(\frac{\mu}{x}\right)^{0.2} \ln\left[1 + \frac{\lambda B_1}{P_r^{2/3}}\right] \qquad (4)$$

This regression rate law is independent of pressure and dependent primarily on the local specific mass flux. Smoot and Price have reported experimental results showing agreement with predicted regression rates for lower values of G.[6,7] For larger values of G agreement was not as good, and a definite pressure effect was found to exist. In another paper the pressure dependence of the regression rate was investigated, and several pressure dependent mechanisms were analyzed.[8] The pressure dependence was considered to be due to heterogeneous reactions.

Returning to Equations 2 and 3, it can be seen that values for two empirical constants must be known to compute the individual heat transfer rates. Estimates for these

constants have been determined from experimental regression rate data. Little data are available to evaluate them from direct measurement of the heat transfer rates. Searle used thin-film thermometers as heat sensors to measure the radiant heat flux to the fuel surface during the hybrid combustion process.[9] His results showed that the method was conceptually sound, but he did not gather sufficient data to draw any firm conclusions. Further information on the magnitude of the heat transfer rates and how they vary as functions of system parameters is necessary to verify the validity of Equation 1. More accurate values for α and β could be found from data obtained by direct measurement of the heat transfer rates. The purpose of this investigation was to study the radiant heat transfer rates using a refined thin-film thermometer technique. The study investigated the variation in magnitudes of the heat transfer rates as functions of oxidizer mass flux and combustion chamber pressure.

1.1 Fuel-Oxidizer Selection

The fuel-oxidizer combination used in this investigation had to be one in which both convective and radiative heat transfer were significant. The essential property of the system is that its combustion products include a large number of particles which will radiate energy. The fuel must be easily obtained. Plastics, such as plexiglass and polystyrene, are readily available and behave similarly to

fuels being considered for use in hybrid rocket motors. A fuel consisting of polystyrene with 0.5 per cent carbon by weight as an additive was selected. Gaseous oxygen was chosen as the oxidizer. This system is considered to be in the "highly radiative" class, as evidenced by direct flame temperature measurements using an optical pyrometer.[10]

1.2 Thin-Film Thermometer Theory

Thin-film thermometers were developed for use in investigating the total heat flux to a surface which was experiencing aerodynamic heating. These thermometers consist of a very thin metal film bonded to a non-conductive substrate material. The history of the surface temperature of the substrate is obtained from changes in the voltage drop across the metal film as its resistance increased with increasing temperature. Vidal found, using simplifications for short test times and thin metal films, that the heating rate may be evaluated by using Equation 5.[11]

$$\dot{Q}(t) = \frac{\sqrt{\pi}\,(\rho_s c_s k_s)^{1/2}}{2}\left\{\frac{T(t)}{(t)^{1/2}} + \frac{1}{\pi\sqrt{t}}\int_0^t \frac{\sqrt{\tau}\,T(t) - \sqrt{t}\,T(t)}{(t-\tau)^{3/2}}\,d\tau\right\} \quad (5)$$

This equation is based on the assumption that for short time periods the substrate material in the thermometer can be considered a one-dimensional semi-infinite body. The performance of the gage is dependent upon the lumped thermal

parameter $(\rho_s c_s k_s)^{\frac{1}{2}}$ of the substrate and the resistance-temperature characteristic ($\Delta R/\Delta T$) of the film. Temperature as a function of time is determined from $\Delta R/\Delta T$ and changes in voltage across the thin-film sensor. If the heat transfer rate is constant, Equation 5 reduces to

$$\dot{Q}(t) = \frac{\sqrt{\pi}\,(\rho_s c_s k_s)^{\frac{1}{2}}}{2}\left\{\frac{T(t)}{(t)^{\frac{1}{2}}}\right\} \qquad (5a)$$

This simplification is justified if the change in voltage across the thin-film resistance is parabolic in shape. An unsteady heat transfer rate can be evaluated by using the entire equation and numerical techniques.[12]

Since the basic thin-film sensor measures the total heat flux to a surface, some modification is required to insure that only radiant heat is being measured. The addition of a transparent covering will prevent the device from being exposed to non-radiant energy. Bogden has investigated the performance of radiant flux meters made utilizing various materials.[13] If the heat sensor is to be used in tests of long duration, a shutter arrangement is required to provide short heat pulses. The design and operation of such a radiant flux sensor was reported by Hardy and Paddock.[14]

1.3 Radiation from Flames and Particles

Selecting a suitable transparent window for a heat sensor to measure the radiation from a combustion zone required knowledge of the wave lengths emitted during the

combustion process. Gases such as hydrogen and oxygen have symmetrical molecules and do not contribute significant amounts of radiant energy. On the other hand polyatomic species such as carbon dioxide, carbon monoxide, and water vapor can be expected to make contributions to the radiant flux.[15] High temperature carbon particles that are formed as the fuel decomposes are believed to contribute most of the radiant energy transport to the fuel surface in the system studied. A black body radiation distribution can be assumed for this portion of the radiant energy transport, since the spectra of high temperature carbon particles is dependent upon the number of atoms in the cluster. A similar assumption can be made for fuels with metal additives. Gases such as carbon dioxide have discrete emission spectrums, and the assumption of a black body distribution is not justified.

The temperature of the flame in the combustion process used for this investigation was in the neighborhood of $2600^{\circ}K$.[4] At this temperature, comparison of the relative magnitudes of the irradiance from the spectral bands of carbon dioxide shows that wave lengths less than 3.0 microns contribute most of the energy.[16] A similar comparison for carbon monoxide and water vapor can be made. Since the black body radiation distribution at $2600^{\circ}K$ has a maximum at a wave length of 1.1 microns, it can be reasonably assumed that 80 per cent of the radiant energy will come from wave lengths less than 3.0 microns. The previous discussion

indicates that a suitable window for a radiant heat sensor to be used in examining irradiance from a combustion zone would be one whose transmittance is high for wave lengths up to 3.0 microns. Materials satisfying this requirement include sapphire, quartz, and some types of glass.[17]

SECTION 2

INSTRUMENTATION AND APPARATUS

2.1 Heat Sensor Design

Designing an instrument to measure the radiant heat transfer rates to a regressing fuel grain presented many problems. The conditions in the combustion chamber require that any form of instrumentation used in the chamber be able to withstand the rigors of a high-temperature oxidizing environment. Searle successfully adapted the thin-film thermometer for use as a heat sensor to measure the radiative portion of the energy transport.[9] He found, however, that an individual sensor could not survive for more than a few experiments. Searle also encountered difficulty in achieving rapid total exposure of the entire sensor face in a short time period. Rapid exposure of the gage face is required to permit use of Equation 5a in evaluating the sensor signal. Commercially manufactured thin-film thermometers of a suitable nature for use in this type of investigation would be expensive. Since a large number of the sensors were required for the planned experimental program, development of a local capability to manufacture suitable heat sensors was necessary.

A sensor face diameter of 0.25 inches was selected as a starting point for sensor construction to increase the probability of achieving rapid exposure of the sensor.

Initially, it was hoped that a single sensor could be developed which would record both total and radiative heat transfer rates simultaneously. Such a sensor might consist of a film on an optically transparent substrate material of low thermal conductivity which would measure the total heat transfer rate. This film would then be placed over a similar film which would measure the radiant energy. Development of a dual element sensor was abandoned when difficulty was encountered in obtaining a suitable single element sensor.

Consideration must be given to the resistance of the metal film used as a thin-film thermometer. Film resistances which are too low invalidate the assumptions Vidal used in developing Equation 5. Vidal indicates that film resistances of at least 20 ohms are required for films whose length is approximately equal to 0.25 inches.[11] Two methods can be used to apply the metal film to the substrate material. These methods are vacuum deposition of the metal and application of a metal paint to the substrate material. After a film of appropriate resistance is obtained, its reflectivity must be evaluated if it is to be used to measure radiant energy. This problem is usually solved by applying a coating of known absorbtivity over the film. Several commercially made carbon black solutions are available for this purpose.

Evaluation of the data from a thin-film thermometer requires knowledge of the thermal parameter (ρ c k) of the

substrate material. This parameter is well known for substrate materials such as quartz, plate glass, and pyrex glass. Pyrex glass #7740 exhibits a high degree of uniformity among specimens.[18] This material was chosen as the substrate material for the heat sensors manufactured for this investigation. The value of $(\rho_s c_s k_s)^{\frac{1}{2}}$ for pyrex #7740 has been reported to be between 0.0737 and 0.0743 $BTU/ft^2 sec.^{\frac{1}{2}}$ [19] A value of 0.0737 was chosen to evaluate the data from heat sensors constructed for this investigation.

Transparent windows made from Corning #7940 fused silica were purchased for use in manufacturing the sensors. As can be seen from Figure 2, the transmissivity of this material is nearly constant up to wave lengths of 3.0 microns. For a window 0.0625 inches thick, the thickness of those used in the heat sensors, 93 per cent of the radiant energy will be transmitted.

The heat sensors had to be mounted through the walls of the combustion chamber. The film-substrate assemblies were encased in a hollow cylinder constructed from paper phenolic. This provided a finished heat sensor which was easily fitted into a pressure tight fitting. It was expected that some deterioration of the phenolic would occur during each experiment. Details of each step taken in manufacturing the heat sensors are included in Appendix A. Photographs of completed sensors appear in Figures 3 and 4.

2.2 Apparatus

The hybrid rocket test apparatus used for the experiments was initially designed and constructed by Lousma at the Naval Postgraduate School.[20] Searle later designed and added the slab burner.[9] Only the slab burner assembly and associated supply and control systems were used for this investigation. No major changes were made in the burner which is described in Reference 9. The time between successive experiments was reduced by constructing 3 new fuel holders which would accommodate the smaller heat flux instrumentation utilized. A photograph of the burner and a fuel holder appears in Figure 5.

The slab burner assembly had been designed to withstand an internal pressure of 1000 psig. Armstrong DC-100 gasket material was used to seal the assembly. The bolts holding the assembly together were torqued to 150 in-lbs to insure a proper seal. The exhaust nozzle consisted of a graphite insert cooled with water. The pressure in the burner was a function of the area of the orifice in the nozzle insert and the oxidizer mass flow rate. Mass burning rates found by Searle were used to obtain estimates of the total mass flow and the orifice diameters required in the insert.

Various systems supplied oxygen, nitrogen, ignition fuel, and coolants to the burner assembly. The oxidizer system supplied both main and ignition oxygen. A purge system supplied nitrogen to the burner. Electrical power and ignition fuel were provided by the ignition system.

All of the fluid supply systems were controlled by solenoid valves. A schematic drawing of the systems is shown in Figure 6.

The oxidizer system consisted of a three bottle gas manifold and associated control valves. A Victor Equipment Company Model GD-10 regulator controlled the pressure of the oxygen. Supply pressures of 0 to 500 psig at flow rate of up to 25 SCFM were possible. Oxidizer flow rates were controlled with calibrated sonic chokes. The chokes available had throat diameters of .081, .1068, .1368, and .191 inches. A plot of plenum chamber pressure versus flow rate was available in Reference 20. The flow from the supply bottles to the plenum chamber was assumed to be adiabatic.

Nitrogen for the purge system was supplied from a two bottle manifold and a Victor Equipment Company Model SR-2BH regulator. Compressed air was blown through the combustion chamber after each firing to cool the assembly. Ignition fuel was supplied directly from a small commercial propane bottle, and primary electrical power for the ignition spark was 115 volt, 60 cycle A.C.

The control panel for operating the apparatus was located in the control room of the Naval Postgraduate School's Rocket Laboratory. The control system was designed to minimize the operations required of the experimenter. The use of spring and solenoid controlled switches in the control panel permitted this ease of operation. A circuit diagram of the control panel is shown in Figure 7. The

circuits permitted simultaneous activation of purge nitrogen and cut off of main oxidizer flow. This minimized burning rate caused by time differences between oxidizer flow cut off and the end of combustion.

2.3 Instrumentation

Instrumentation requirements for the investigation were not extensive. Two pressure measurements and a record of the heat sensor voltage level were the only data outputs requiring installation of instrumentation. A Honeywell Model 1508 visicorder was available as part of permanent instrumentation in the Rocket Laboratory, and it was used to record these data outputs. The use of the visicorder provided a record of this data on one strip chart. Schematic representations of the circuits used to transmit the instrumentation output signals to the visicorder are seen in Figures 8 and 9.

A pace Model CP-40A, 0-600 psia, transducer was installed to measure the pressure in the plenum chamber. This transducer was installed in parallel with a Marsh Master Pressure Gage Model 200-4S. The output of the transducer was fed into a Honeywell Series M subminiature galvanometer. The galvanometer's sensitivity was adjusted to 100 psig per inch through the use of a 50 kilo-ohm potentiometer across the transducer output. Combustion chamber pressure was obtained similarly using a Wianko Type P2-3086, 0-300 psig transducer. Galvanometer sensitivity in this case was 50

psig per inch. An Ashcroft Model 1172BB provided visual monitor of chamber pressure. The direct reading pressure gages were located such that they could be observed by the control panel operator.

The heat flux measurement circuit is shown in Figure 9. It was assumed that the current I_h, which flows in the heat sensor, was constant. This assumption was justified because changes in the heat sensor resistance were small compared to the large 20,160 ohm current limiting resistance in the circuit. A change of 100 ohms in sensor resistance caused a change of only 0.5 per cent in I_h. The impedance of the Astro Data 885 Differential Amplifier was greater than 100 megohms, making it appear as an open circuit to the power supply. A power supply voltage of 10.1 volts was required to provide an I_h of 0.5ma. It was desirable to dissipate as little energy as possible in the heat sensor, thus the excitation current was minimized. For a sensor current of 0.5ma, the rate of heat dissipation in a 100 ohm resistance equals 2.37×10^{-9} BTU/sec. This heat dissipation rate was small, and hence, the temperature of the sensor was never significantly above that of the surrounding fuel.

Changes in the voltage across the heat sensor were amplified and then fed to a Honeywell M400 galvanometer. The steady state voltage from the sensor was sufficient to force the galvanometer off scale with amplification factors of ten or more. The steady state voltage at the input to the amplifier was reduced to zero by applying a voltage of

reverse polarity using a six volt battery. The current flowing in the signal return portion of the circuit was small, and no significant error in the sensor signal was caused by the bucking voltage circuit resistance. A full analysis of the heat sensor circuit appears in Appendix B. A visicorder paper speed of 10 inches per second provided a trace from which sensor voltage as a function of time could be determined. By utilizing this information, the heat transfer rate was computed using Equation 5a.

It was decided that sufficiently accurate regression rate information could be determined by the measurement of thickness changes near the thin-film sensor. Fuel mass burning rate was determined by recording the weight changes during each firing. Both of these measurements required an accurate record of the time duration of each firing. By recording the trace of a 20 cps signal on the strip chart, the time of burning was then determined by counting the number of cycles between the rise of oxygen pressure in the plenum chamber and its return to zero. Errors caused by the small amount of fuel consumed during ignition were not considered great enough to warrant the use of methods giving greater accuracy.

2.4 Instrumentation Calibration

The pressure transducers were calibrated after being installed as part of the apparatus. The Marsh Master Pressure Gage was used as a standard pressure reference.

This gage and the smaller Ashcroft gage were calibrated prior to installation by the calibration facility at Alameda Naval Air Station, Alameda, California. Calibration of the transducers was accomplished by sealing the combustion chamber and then pressurizing it with nitrogen. After observing the pressure indicated by the standard gage, the deflection of the galvanometer was adjusted using the potentiometer. Both transducers were linear throughout the expected range of pressures. Figure 10 shows the calibration curves used during the experiments.

The value of $\Delta R/\Delta T$ for each thin-film thermometer was determined by recording steady state voltages at temperatures between 70 and 280^{o}F. A circuit similar to the one installed as part of the experimental apparatus was constructed to perform the calibration. An integrating digital voltmeter replaced the amplifier-visicorder portion of the circuit. The temperature of the film was determined with a thermocouple which had been mounted in the center of an aluminum block. Figure 11 shows a cross section of the arrangement. The block was placed on an electric hot plate such that one surface was heated at a uniform rate. The resistance of the film at a given temperature was computed from the voltages recorded. Figure 12 illustrates typical plots obtained. All of the films calibrated possessed linear $\Delta R/\Delta T$ characteristics. Sensors which had higher room temperature resistances were more sensitive. The resistance of thin metal films changes due to aging.[11] To

establish that the sensor calibration curves remained valid over a period of time, several of the sensors were calibrated twice. No significant change in the $\Delta R/\Delta T$ characteristics was noted over a time interval of seven days.

Calibration of the heat sensor circuit installed in the rocket laboratory was accomplished in the following manner: Small D.C. voltages of various magnitudes were applied to the input of the amplifier. The deflection of the galvanometer was then recorded for three amplification factors. Figure 13 shows the result of this procedure. The circuit was linear and gave repeatable outputs.

SECTION 3

EXPERIMENTAL PROCEDURE

All of the fuel samples were prepared before beginning the experiments. The samples measured 0.25 by 1.4 by 7.0 inches when completed. A completed fuel slab appears in Figure 14. The leading edge of each slab was tapered to insure a smooth flow of oxygen on the burning surface. At a distance 4.625 inches from the leading edge of the slab, a recess 0.31 inch in diameter and 0.125 inch deep was drilled to allow insertion of the heat sensor into the fuel slab. The bottom of the recess was made slightly deeper around its circumference. Initially this was not done; but when early test results indicated that the sensors were not uncovering as rapidly as desired, the procedure was tried and the data improved. Finally, four 0.125 inch holes were drilled so that small plastic rods could be inserted to hold the fuel to the metal holder. Each slab was weighed to the nearest 0.01 gram, and its thickness 4.625 inches from the leading edge was measured using a micrometer. This information was recorded for use later in burning rate determination.

Three samples were installed in the holders each day for use in the following day's experimentation. To prevent the fuel from burning between the slab and the holder, the back of the slab was coated with General Electric RTV Silicone Rubber. To facilitate removal of the inhibiting

material from the slab following the experiment, a piece of masking tape was placed on the fuel before applying the RTV. After fitting the slab into the holder and insuring that the heat sensor recess was free of RTV, the plastic pins were inserted.

Daily laboratory routine began by turning on all of the instrumentation. During the warm up period, data sheets were prepared for the planned experiments, and preparations for the first experiment were completed. Prior to installing a fuel slab and holder in the combustion chamber, a disk of aluminum foil was placed in the bottom of the recess in the fuel slab. The foil functioned as a small heat sink which protected the sensor from excessive pre-heating and promoted more even burning of the fuel above it. Additionally, the foil acted as a "shutter" which increased the rate of sensor exposure. The completed fuel holder and fuel slab assembly were installed, and the side of the combustion chamber was bolted in place.

A check was made prior to each experiment to insure that the heat sensor and its associated instrumentation were operating properly. After allowing the sensor to warm up, the check was performed by rapidly exposing the face of the sensor to a 650 watt photo flood lamp. The lamp provided an essentially constant radiant energy flux to the sensor, and proper operation of the instrument was assumed if the visicorder trace was parabolic in shape. If the sensor functioned correctly, it was installed in the chamber.

During the early experiments, two heat sensors sustained damage along the sides of the phenolic holder during the firing cycle. The damage was caused by hot gases in a void area below the fitting used to seal the sensor in the chamber. Figure 15 shows a sensor damaged in this manner. Recurrence of this difficulty was prevented by coating the sensor with RTV and packing the void with asbestos waste. Reference to Figure 17 illustrates the entire assembly in its final configuration.

To verify that the oxygen regulator was delivering the required pressure to the metering orifice, the oxidizer system was activated for approximately two seconds prior to each experiment. This procedure also provided a check of the operation of the pressure transducers. The visicorder trace was compared with the pressure noted on the direct reading pressure gages. Final adjustments were made, and the spark plug was tested for normal operation. At this point, the propane supply was activated. The final step in preparing an experiment was to adjust the heat sensor signal at the amplifier input to zero.

The firing sequence began with simultaneous activation of the ignition switch and visicorder paper drive. After approximately one second, the main oxidizer supply valve was opened. After a rapid change in the heat sensor voltage level was noted, the nitrogen purge system was actuated. Cooling air was then supplied to the chamber for about ten minutes. When the chamber was cool, it was disassembled, and preparations for another run were begun.

Upon completion of three experiments, the partially burned fuel slabs were removed from the holder, cleaned, and weighed to the nearest 0.01 grams. The thickness 4.625 inches from the leading edge was measured using a micrometer. This information, along with any indication of unusual occurrences, was recorded on the data sheet for each experiment.

SECTION 4

DISCUSSION OF RESULTS

A total of twenty-two experiments were performed. This total was approximately half of the originally planned experimental program. The experimental program was reduced because the sensors could not be re-used as many times as was anticipated. The data obtained from each experiment were recorded on the visicorder strip chart and the data sheet for each experiment. A tracing of a typical strip chart record is shown in Figure 18. The raw data, when reduced, yielded three types of information: fuel mass burning rate, linear regression rate, and radiant heat transfer rate. Sample calculations, showing details of the data reduction procedure, appear in Appendix C. Table 1 summarizes the significant experimental results obtained. The data obtained were separated into two areas, burning rate data and heat transfer information, for convenience in presenting the results. A brief discussion of the performance of the heat sensors is included.

Reduction of the data began by determining the pressure in the plenum and combustion chambers. This was done by measuring the transducer signal recorded on the strip chart and then determining the pressures from the calibration curves for the transducers (Figure 10). The ratio P_b/P_o was calculated to establish that sonic conditions had existed in the metering orifice. Oxidizer mass flow rate

($\dot{m}_o$) was determined by using the calibration curve in Reference 20 for the metering orifice used during the experiment. This preliminary information established the conditions which had existed during the experiment under consideration, specifically the values of $\dot{m}_o$ and P_b. Oxidizer mass flux (G_o) is a parameter normally used in evaluating hybrid combustion data. This parameter was determined by dividing oxygen mass flow rate by the area of the flow channel. For the slab burner, this area was 0.675 square inches at the time the heat sensor was exposed. Data points were obtained for two values of G_o, 0.15, and 0.24 lb_m/in^2sec. The actual values of G_o for all the experiments were within 3 per cent of these values.

4.1 Burning Rate Data

The duration of each firing was determined by counting the number of cycles of the 20 cps signal which occurred while a steady state pressure existed in the plenum chamber. Linear regression rate ($\dot{r}$) was computed by dividing the change in thickness of the fuel slab by the burning time for the experiment. Eleven data points were obtained for an oxidizer mass flux of 0.15 lb_m/in^2sec. These results are shown in Figure 19. The linear regression rates obtained for G_o equal to 0.24 lb_m/in^2sec. are also shown in Figure 19. Only five points for this value of G_o were obtained. No attempt was made to fit a curve to the data for this value of G_o.

Fuel mass burning rate ($\dot{m}_f$) was computed by dividing the change in weight of the fuel slab by the burning time. This information was used to calculate a second linear regression rate ($\dot{r}_c$). The computation was accomplished using Equation 6:

$$\dot{r}_c = \frac{\dot{m}_f}{\rho_f S} \tag{6}$$

The burning surface area (S) used in computing $\dot{r}_c$ was equal to 9.1 square inches. This value was selected as an average burning area during the burning time. The results are also plotted in Figure 19. The computed regression rates were in general larger than those found by direct measurement. This difference was due to variations in the burning surface area. As can be seen from Figure 16, the fuel burned unevenly in the vicinity of the plastic pins. It was felt that the regression rates determined by direct measurement of the fuel slab thickness were more indicative of the actual regression rates.

The linear regression rates obtained during this investigation were compared with those obtained using similar values of G_o by Lousma.[21] The values of the regression rates compared favorably, and the same trends were indicated.

4.2 Heat Sensor Performance

Although useful heat transfer data were obtained, the performance of the heat sensors was not entirely satisfactory. Some deterioration of a sensor was expected during each experiment. Experience showed this to be true; in fact, in some cases the deterioration was significant enough to render the sensor useless after only one experiment. This usually occurred because the viewing window of the heat sensor was lost before the end of combustion. Figure 15 shows a sensor damaged in this manner. Although every effort was made to end the combustion process as soon as an indication that the sensor had been exposed was noted, all of the sensors were eventually rendered useless.

Attempts to rebuild the damaged sensors met with little success. Only one sensor operated satisfactorily after being repaired by replacing the window. Several of the sensors could not be repaired because the MgF_2 coating was scratched, and its insulating qualities were destroyed. Additional difficulty was encountered when the repaired sensors were recalibrated. In almost every case the new $\Delta R/\Delta T$ characteristic was non-linear. This was apparently due to changes in the properties of the epoxy solder material used to attach the leads to the metal film.

Although the heat sensors which remained intact during an experiment responded favorably to a light pulse, there was some evidence that their performance was degraded. Nearly all of the useful heat transfer data were obtained

from instruments which had not previously been used. The use of epoxy resin materials in sensor construction was probably responsible for this trend. For future investigations of a nature similar to this one, sensors constructed utilizing ceramic materials might prove more reliable.

4.3 Heat Transfer Data

The primary objective of this investigation was to measure the radiant energy flux to the surface of the pyrolizing fuel. Prior to calculating the heat transfer rates using Equation 5a, which is applicable only for a constant heat transfer rate, each visicorder trace was examined. Nearly 60 per cent of the traces obtained were not parabolic and could not be used to obtain heat transfer information. These traces generally showed a slow rise in sensor temperature with time. This condition indicated the sensor had not been exposed rapidly enough. Two phenomena, uneven burning of the fuel and soot deposition, probably caused this condition. Soot particles have a high absorbtivity, and build up of a thin layer on the transparent window would prevent transmission of the radiant energy to the substrate surface.

Only those traces which were parabolic in shape were used to calculate the heat transfer rates. These traces remained parabolic for a period of 25 to 50 milli-seconds. This portion of the trace was used to calculate the radiant energy flux measured by the sensor ($\dot{Q}_g$). The change in

sensor voltage was determined utilizing the calibration curve for the heat sensor circuit. Equation 7 was then applied to determine the change in the surface temperature of the sensor substrate.

$$\Delta T = \frac{\Delta V}{I_h (\Delta R/\Delta T)_{sensor}} \tag{7}$$

The time required for this temperature change to take place was determined from the timing trace. Equation 5a was then utilized to calculate the radiant energy flux incident to the substrate surface. This value of the radiant flux was corrected for window transmissivity and sensor reflectivity by applying the following equation

$$\dot{Q}_r = \frac{\dot{Q}_g}{(0.89)(0.93)} \tag{8}$$

In Equation 8, 0.89 was the absorbtivity of the carbon black coating on the sensor face, and 0.93, the transmissivity of the window.

Nine values for the radiant energy flux were obtained at various values for G_o. These data, along with the data obtained by Searle in Reference 9, are plotted in Figure 20. The experimental scatter present in the data made the radiant flux appear to decrease and then increase with increasing pressure. Any conclusions based on this trend would not be justifiable. Radiating particles in the gas stream probably produced most of the radiant flux. Since the particle density (n) can be expected to increase with

pressure, the radiant flux should increase as the pressure increases. The curves in Figure 20 were drawn utilizing a least squares fitting procedure. The slope of the curves indicated that radiant energy flux does increase with pressure.

The data from Reference 9 were somewhat less than the data obtained in this investigation. This difference was probably due to differences in the instrumentation utilized. The smaller heat sensors used for this investigation increased the probability of achieving rapid sensor exposure and decreased the effects of soot deposition. Also the sensors used in these experiments were coated with a carbon black solution. This method of accounting for sensor reflectivity firmly established the correction applied to $\dot{Q}_g$. Searle used experimental data from Reference 13 to correct for sensor reflectivity.

Another trend indicated by the least squares fit of the data was that radiant energy flux decreases slightly as G_o increases. This trend was not well defined, and detailed knowledge of the physical phenomena involved in polystyrene-oxygen combustion would be required to confirm this observation. Further indication of the trend was found from values of αnz calculated by inverting Equation 3 and utilizing the values of the radiant flux obtained. For this calculation T_r was assumed equal to 2100°K and ϵ_w was assumed to be 0.90. The results of the calculations are tabulated in Table 2. Figure 21 shows the results plotted

as a function of pressure. A least squares fit was again used to draw the curves. The lower curve indicated a definite decrease in α_{nz} as G_o increased.

During the course of the experiments, a value of the total heat transfer rate to the fuel surface was obtained when a sensor window was lost prematurely. This value was 83.60 BTU/ft^{2}sec. An estimate of the accuracy of this observation was obtained by computing an effective heat transfer rate using Equation 9 and the regression rate for that experiment, assuming that h_{eff} had a value of 900 BTU/lbm.

$$\dot{Q}_{eff} = \dot{r}\, \rho_f\, h_{eff} \tag{9}$$

The calculation yielded a value for $\dot{Q}_{eff}$ of 117.306 BTU/ft^{2}sec. The large difference noted was probably due to disturbances in the gas flow, since the sensor surface was located at the bottom of the recess left in the fuel surface when the window was lost.

An estimate of accuracy of the values for the radiant energy flux was obtained by calculating $\dot{Q}_{eff}$ for two of the runs for which $\dot{Q}_r$ was obtained. The results are tabulated below.

Run	$\dot{r}$	$\dot{Q}_{eff}$	$\dot{Q}_r$	$\dot{Q}_c$
12	0.0257	128.270	13.419	125.5
17	0.0255	127.312	11.450	126.8

$\dot{Q}_r$ was approximately 10 per cent of the effective heat transfer rate in both cases. In the above table $\dot{Q}_c$ was calculated using Equation 10 and iterating.

$$\dot{Q}_{eff} = \dot{Q}_r + \dot{Q}_c e^{-\frac{\dot{Q}_r}{\dot{Q}_c}} \tag{10}$$

Equation 1, from which Equations 9 and 10 were derived, indicates that the two modes of heat transfer are physically coupled. An increase in the radiant flux increases the rate at which mass leaves the fuel surface. This increased mass flux from the fuel surface acts to block the convective heat transfer to the fuel surface. For fuels which have low metal loading, this trade-off is approximately one.[5] The calculations above verified this and add credence to the form of Equation 1. The results also indicated the obtained values for the radiant energy flux were probably reasonably accurate.

SECTION 5

CONCLUSIONS

The data obtained established a range of 10 to 14 BTU/ft^2sec for the radiant flux to the fuel surface during hybrid combustion of the polystyrene-oxygen system. This range was established for oxidizer mass fluxes of 0.15 and 0.24 lbm/in^2sec and combustion chamber pressures from 7 to 14 atmospheres.

Utilizing the linear regression rates obtained, values for the effective heat transfer rate to the fuel surface were calculated. These values and the measured values of the radiant energy flux were used to obtain values for the convective heat transfer rate to the fuel surface. The calculations appeared to verify Marxman's analytical formulation for the linear regression rate in terms of the physical coupling between the convective and radiative heat transfer rates.

An apparent increase in radiant energy flux with increased pressure was believed to be the result of an increase in the density of radiating particles in the gas stream. A decrease in radiant energy flux with increasing oxidizer mass flux was noted. Further experimental data would be required to establish the validity of this observation.

The use of thin-film thermometers as a heat sensing device to measure the radiant flux to a pyrolyzing fuel

surface was proven conceptually sound. Sensor durability must be improved to increase the rate of data acquisition. Materials which will withstand high temperature should be used in constructing heat sensors to be used in conjunction with this type of experiments.

The selection of a highly radiative fuel-oxidizer system which will not form a large amount of carbon during combustion would be advisable for any further experimental studies of this type. This choice would lessen the possibility of encountering soot deposition of the sensor window.

BIBLIOGRAPHY

1. Green, L., Jr. "Introductory Considerations on Hybrid Rocket Combustion," Heterogeneous Combustion, Progress in Astronautics and Aeronautics, Vol. XV (New York: Academic Press, 1964), pp. 451-484.

2. Penner, S.S. Chemical Rocket Propulsion and Combustion Research (New York: Gordon and Breach, 1962), pp. 145-153.

3. Marxman, G.A., and Gilbert, M. "Turbulent Boundary Layer Combustion in the Hybrid Rocket," International Symposium on Combustion, Vol. IX (Academic Press, 1963), p. 371.

4. Marxman, G.A., Wooldridge, C.E., and Muzzy, R.F. "Fundamentals of Hybrid Boundary Layer Combustion," Progress in Astronautics and Aeronautics, Vol. XV (New York: Academic Press, 1964), pp. 485-522.

5. Marxman, G.A. and Wooldridge, C.E. Research on the Combustion Mechanism of Hybrid Rockets. 25th Meeting of the Combustion and Propulsion Panel, AGARD, NATO, La Jolla, California, 22 to 23 April, 1965.

6. Smoot, L.D., and Price, C.F. "Regression Rate Mechanisms of Non-metallized Hybrid Fuel Systems," AIAA Journal, 3:1408-1413, August, 1965.

7. Smoot, L.D., and Price, C.F. "Regression Rates of Metallized Hybrid Fuel Systems," AIAA Journal, 4:910-915, May, 1966.

8. Smoot, L.D., and Price, C.F. "Pressure Dependence of Hybrid Fuel Regression Rates," AIAA Journal, 5:102-106, January, 1967.

9. Searle, H.D. "Measurement of Radiant Heat Transfer to the Fuel Grain Surface in a Hybrid Rocket Using Thin-Film Resistance Thermometers," Aeronautical Engineer Thesis, Naval Postgraduate School, Monterey, California, 1966.

10. United Technology Center. Investigation of Fundamental Phenomena in Hybrid Propulsion. Quarterly Technical Progress Report UTC 2097-QPR1, September, 1964. (Confidential)

11. Vidal, R.J. Model Instrumentation Techniques for Heat and Force Measurements in a Hypersonic Shock Tunnel. Cornell Aeronautical Laboratory Report AD-917-A-1; WADC TN 56315 AD 97238, February, 1956.

12. Cook, W.J., and Felderman, E.J. "Reduction of Data From Thin-Film Heat Transfer Gages: A Concise Numerical Technique," AIAA Journal, 4:561-562, March, 1966.

13. Bogden, L. Measurement of Radiative Heat Transfer with Thin-Film Resistance Thermometers. National Aeronautics and Space Administration, Contractor's Report No. 27, March 1964.

14. Hardy, R.G., and Paddock, D.A. "A New Thermal Radiative Flux Gage," ISA Transactions, 6:15-19, January, 1967.

15. Hottel, H.C. Chapter 4 of Heat Transmission (By W. C. McAdams), 3rd ed. (New York: McGraw-Hill Book Company, Inc., 1954).

16. Penner, S.S. Quanitative Molecular Spectroscopy and Gas Emissivities (Reading, Massachusetts: Addison-Wesley, 1963), 595 pp.

17. Kruse, P.W., McGlauchlin, L.D., and McQuiston, R.B. Elements of Infrared Technology: Generation, Transmission, and Detection (New York and London: John Wiley and Sons, Inc., 1962), pp. 119-161.

18. Bogden, L. High-Temperature, Thin-Film Resistance Thermometers for Heat Transfer Measurement. National Aeronautics and Space Administration, Contractor's Report No. 26, April, 1964.

19. Bogden, L. "Thermal and Electrical Properties of Thin-Film Resistance Gages Used for Heat Transfer Measurement," AIAA Journal, 1:2172-2173, September, 1963.

20. Lousma, J.R. Design and Operation of a Hybrid Rocket. Naval Postgraduate School, Department of Aeronautics, TN 64T-8, May, 1965.

21. Lousma, J.R. "A Parametric Burning Rate Study of the Polystyrene-Oxygen Hybrid Fuel System." Aeronautical Engineer Thesis, Naval Postgraduate School, Monterey, California, May, 1965. (Confidential)

22. Wooldridge, C. E., and Muzzy, R.J. "Internal Ballistic Considerations in Hybrid Rocket Design," Journal of Spacecraft and Rockets, 4:255-262, February, 1967.

TABLE 1

SUMMARY OF EXPERIMENTAL RESULTS

Run No.	P_b atm	G_o lb_m/in^2sec	$\dot{r}$ in/sec	$\dot{r}_c$ in/sec	$\dot{Q}$ BTU/ft^2sec	
1	10.00	0.120			10.778	
5	10.53	0.145	0.0247	0.0255	9.676	
6	10.10	0.150	0.0271	0.0278		
7	9.67	0.150	0.0240	0.0249		
8	10.00	0.148	0.0275	0.0296		
9	8.53	0.148	0.0213	0.0245		
11	9.00	0.148	0.0264	0.0279	14.220	
12	13.00	0.150	0.0257	0.0278	13.419	
13	12.80	0.151	0.0241	0.0276		
14	12.80	0.151	0.0242	0.0245		
21	7.55	0.148	0.0249	0.0261	11.534	
15	14.15	0.238			13.528	
16	15.30	0.240	0.0384	0.0386		
17	11.13	0.237	0.0255	0.0280	11.450	
19	10.67	0.237	0.0271	0.0275		
20	8.20	0.240	0.0229	0.0291	12.168	
22	12.20	0.238	0.0316	0.0331	10.821	
4	13.53	0.155	0.0253	0.0292	83.600	($\dot{Q}_{total}$)

TABLE 2

CALCULATED VALUES OF α_{nz}

Pressure atm	G_o lbm/in^{2}sec	$\dot{Q}_r$ BTU/ft^{2}sec	α_{nz}
7.55	0.148	11.534	0.139
8.20	0.240	12.168	0.148
9.00	0.148	14.220	0.176
10.00	0.120	10.778	0.130
10.53	0.145	9.676	0.115
11.13	0.237	11.450	0.138
12.20	0.238	10.821	0.130
13.00	0.150	13.419	0.165
14.15	0.238	13.528	0.166

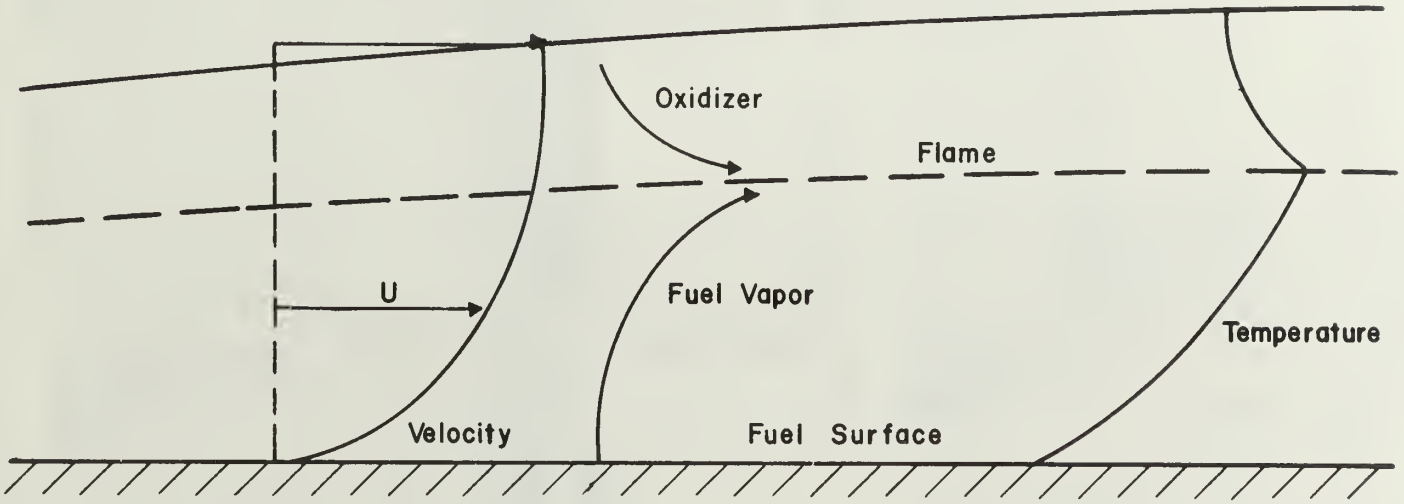

BOUNDARY LAYER COMBUSTION MODEL

FIGURE 1

SPECTRAL TRANSMISSION OF FUSED QUARTZ
(REFERENCE 17)
FIGURE 2

HEAT SENSOR COMPONENTS
FIGURE 3

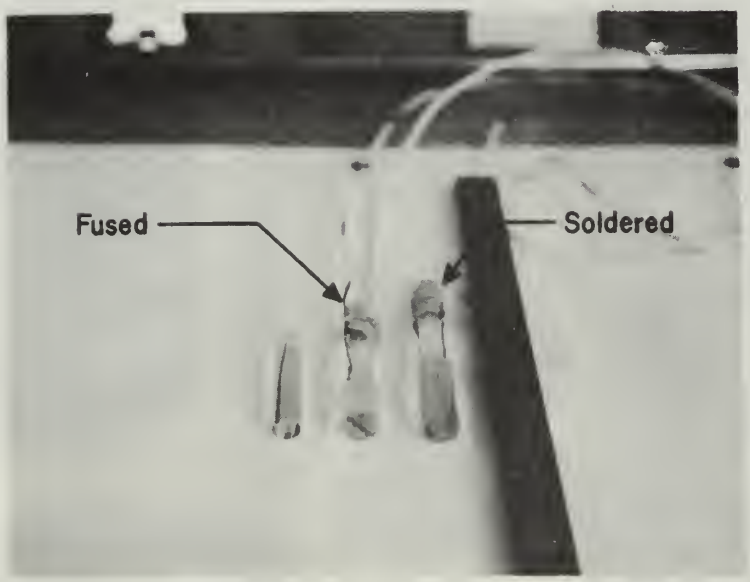

EXAMPLES OF THIN-FILM THERMOMETERS CONSTRUCTED

FIGURE 4

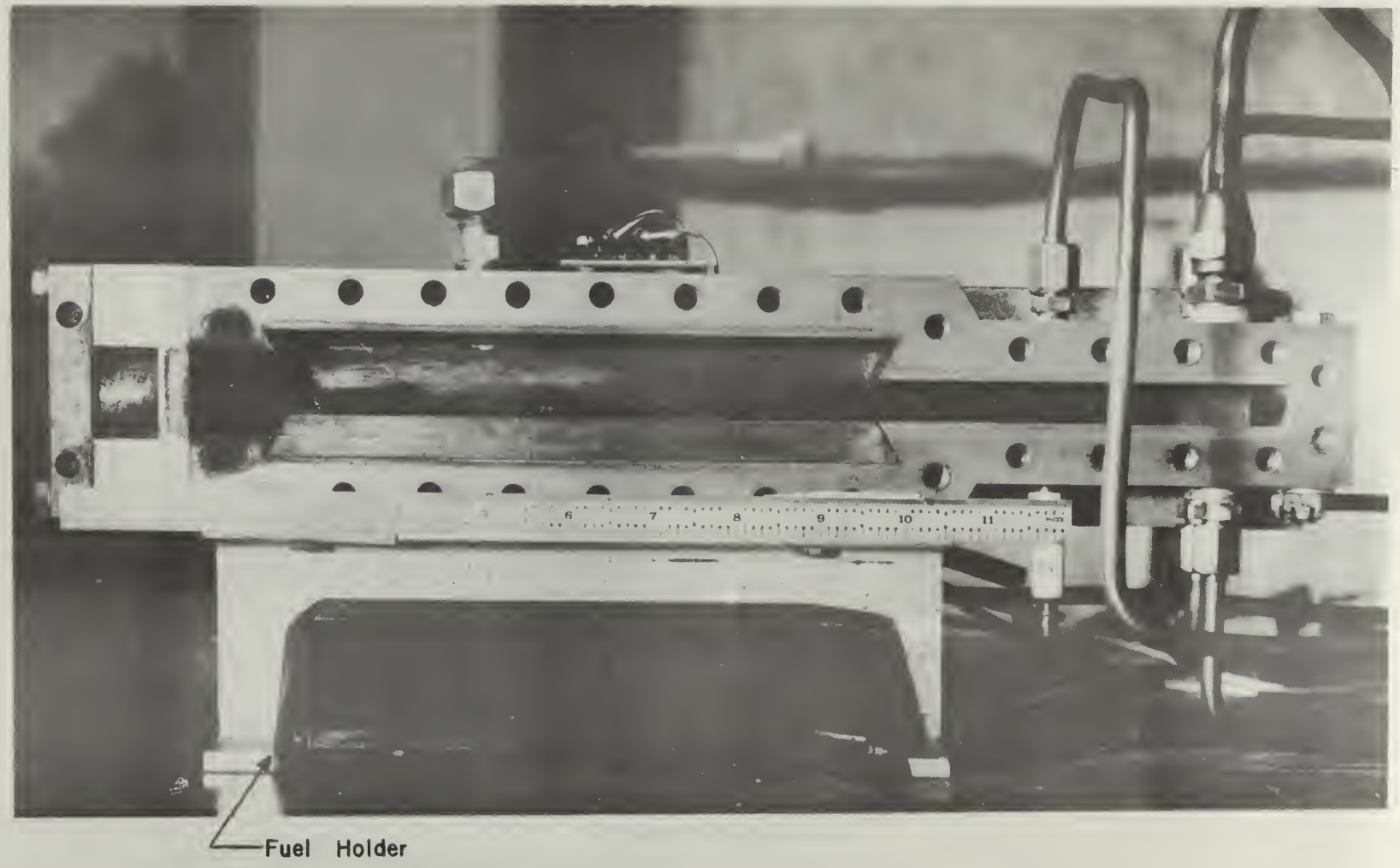

THE COMBUSTION CHAMBER
FIGURE 5

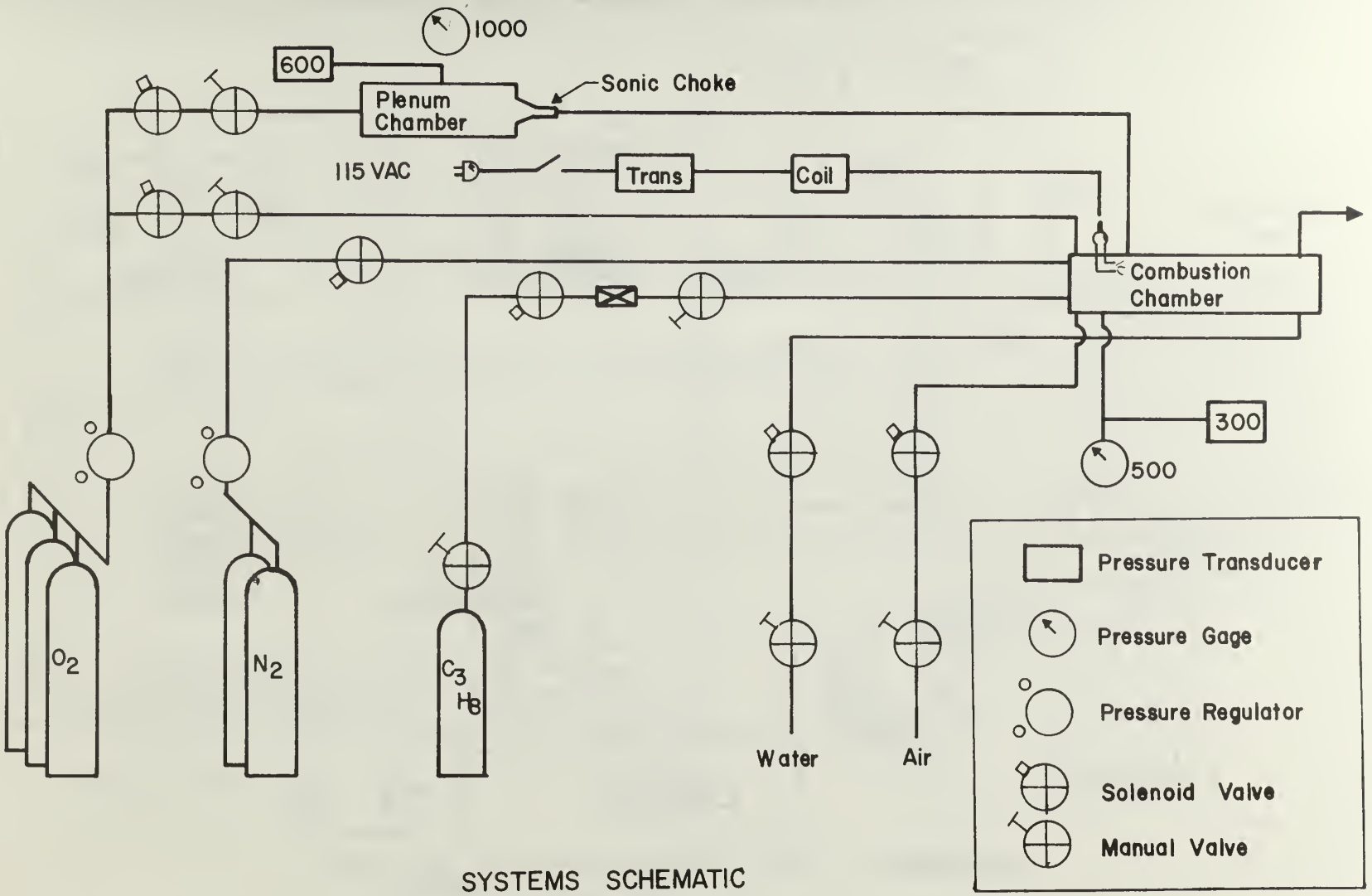

SYSTEMS SCHEMATIC
FIGURE 6

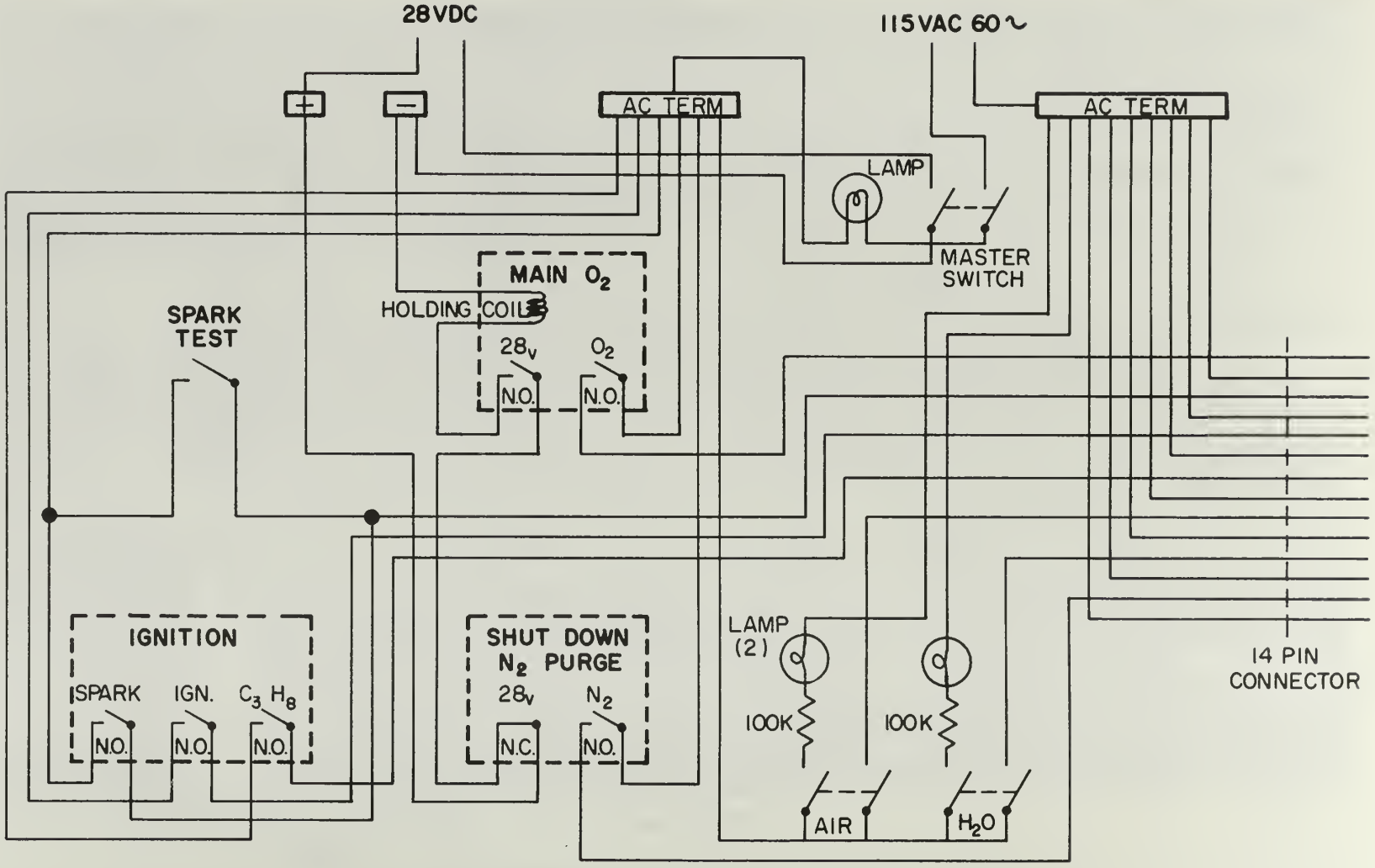

CONTROL BOX CIRCUIT SCHEMATIC
FIGURE 7

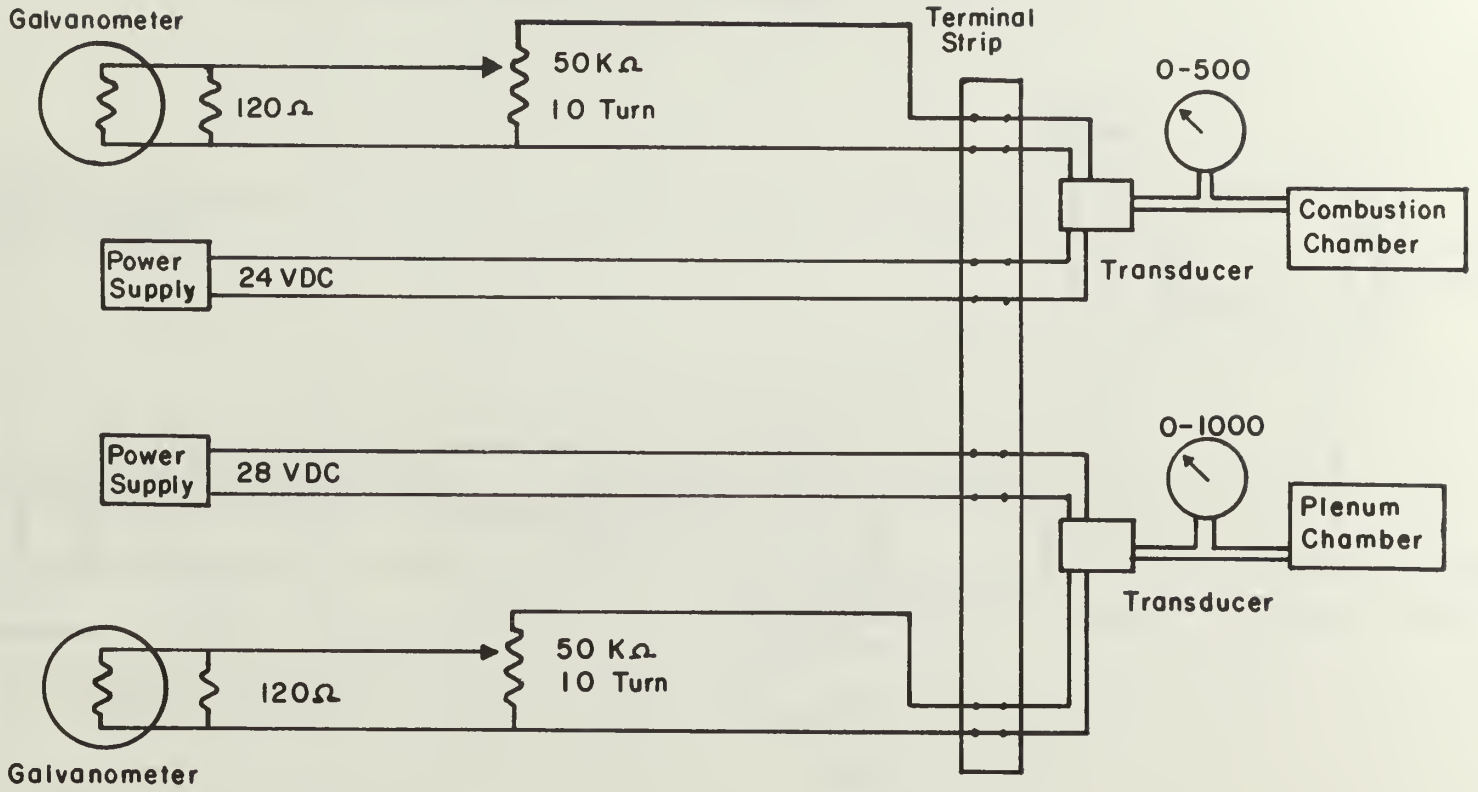

PRESSURE INSTRUMENTATION CIRCUIT SCHEMATIC

FIGURE 8

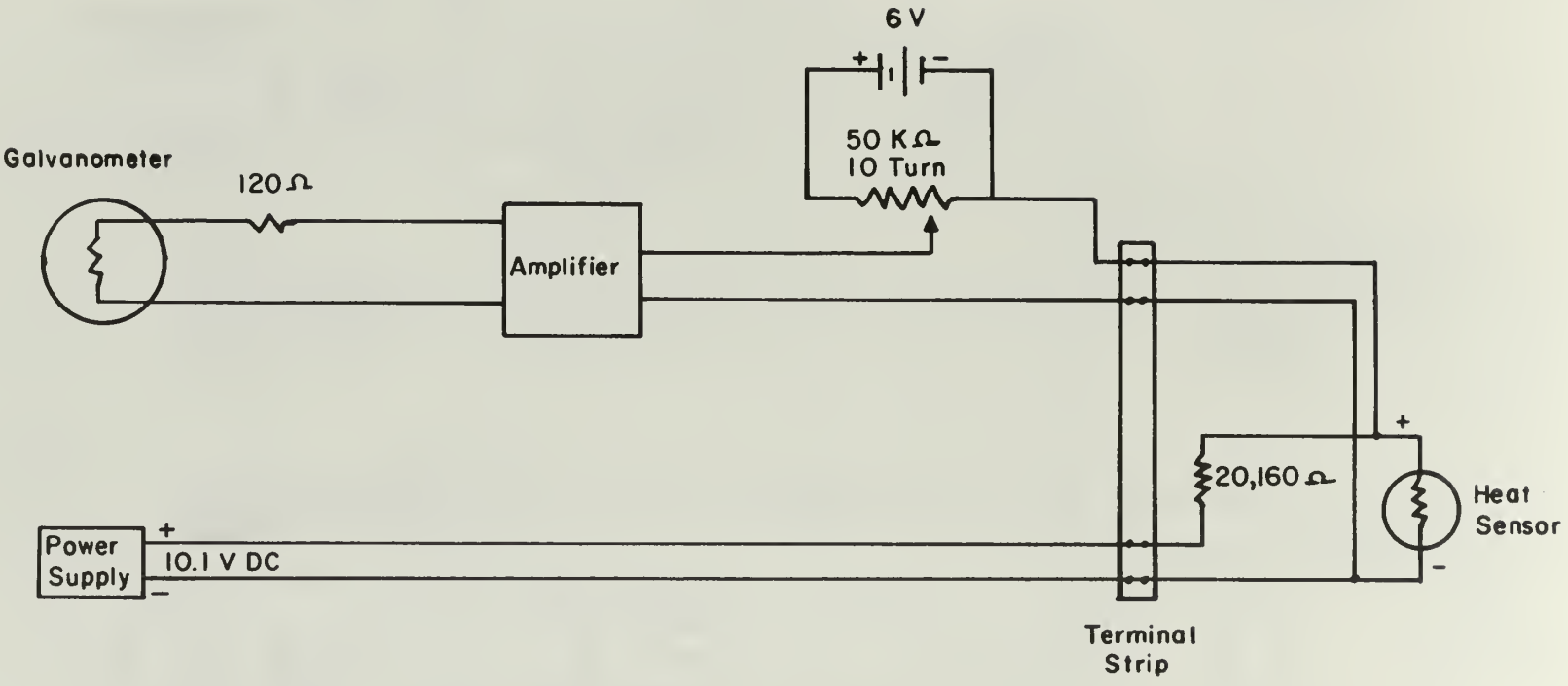

HEAT SENSOR CIRCUIT SCHEMATIC

FIGURE 9

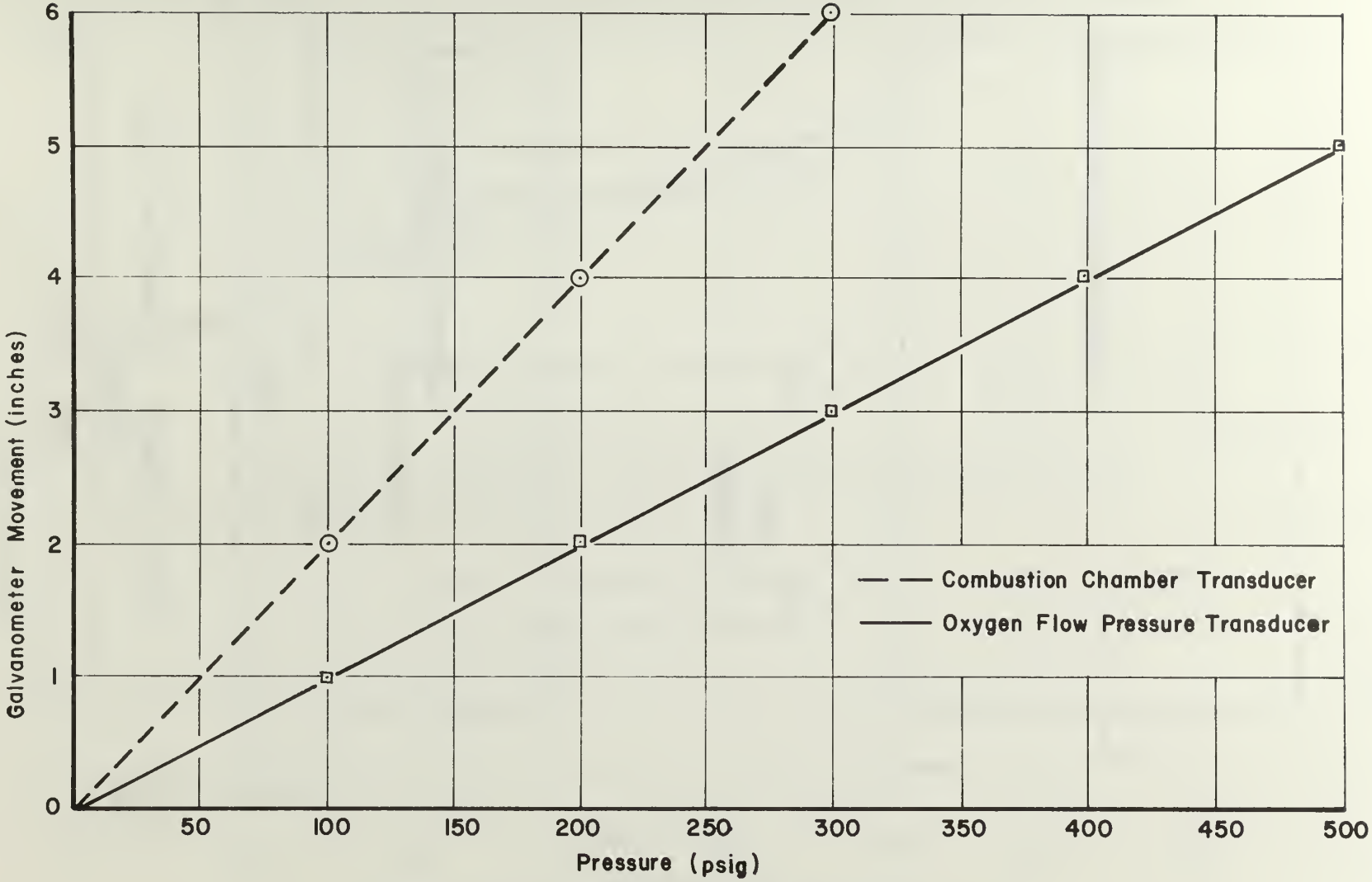

PRESSURE TRANSDUCER CALIBRATION
FIGURE 10

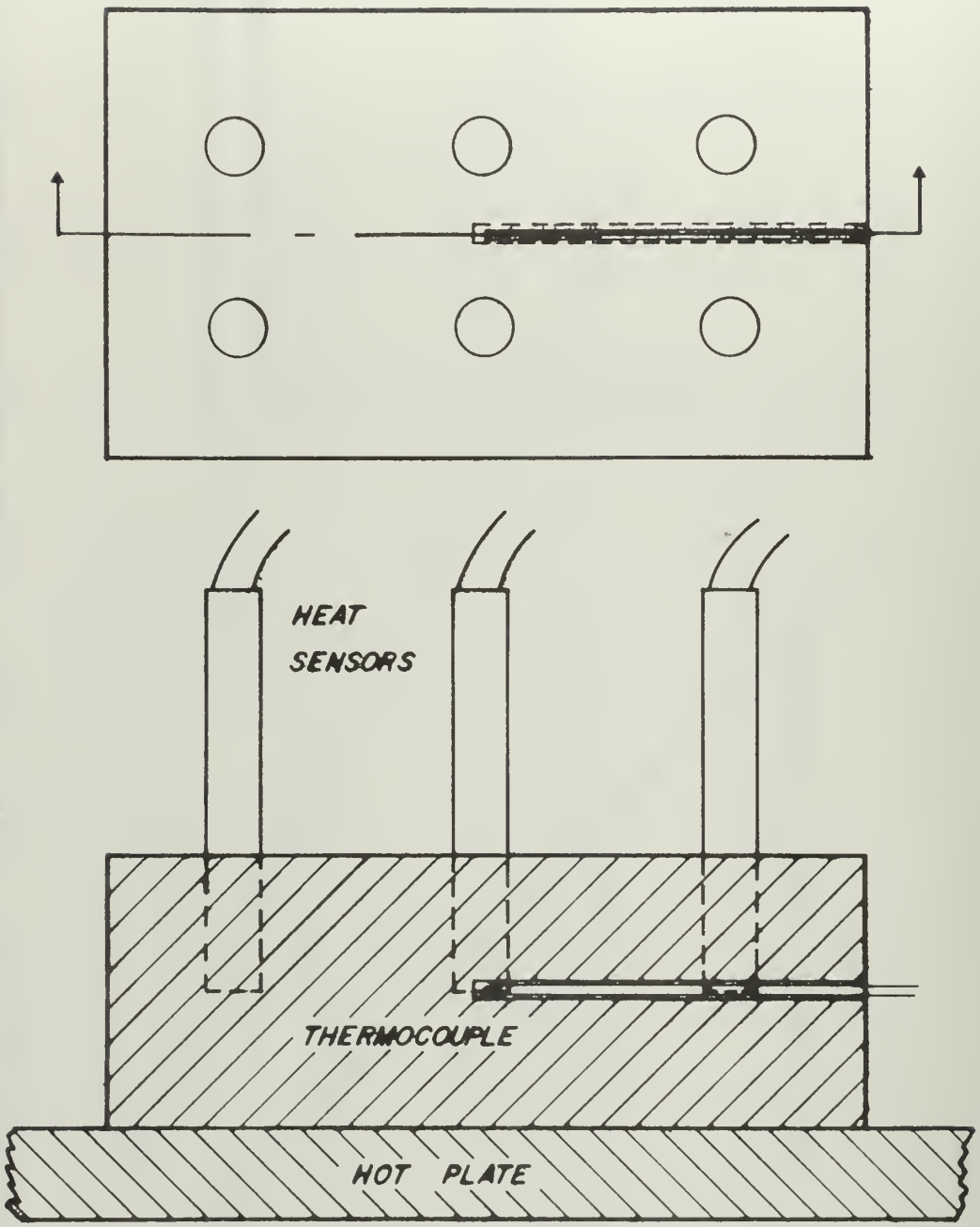

HEAT SENSOR CALIBRATION BLOCK
FIGURE 11

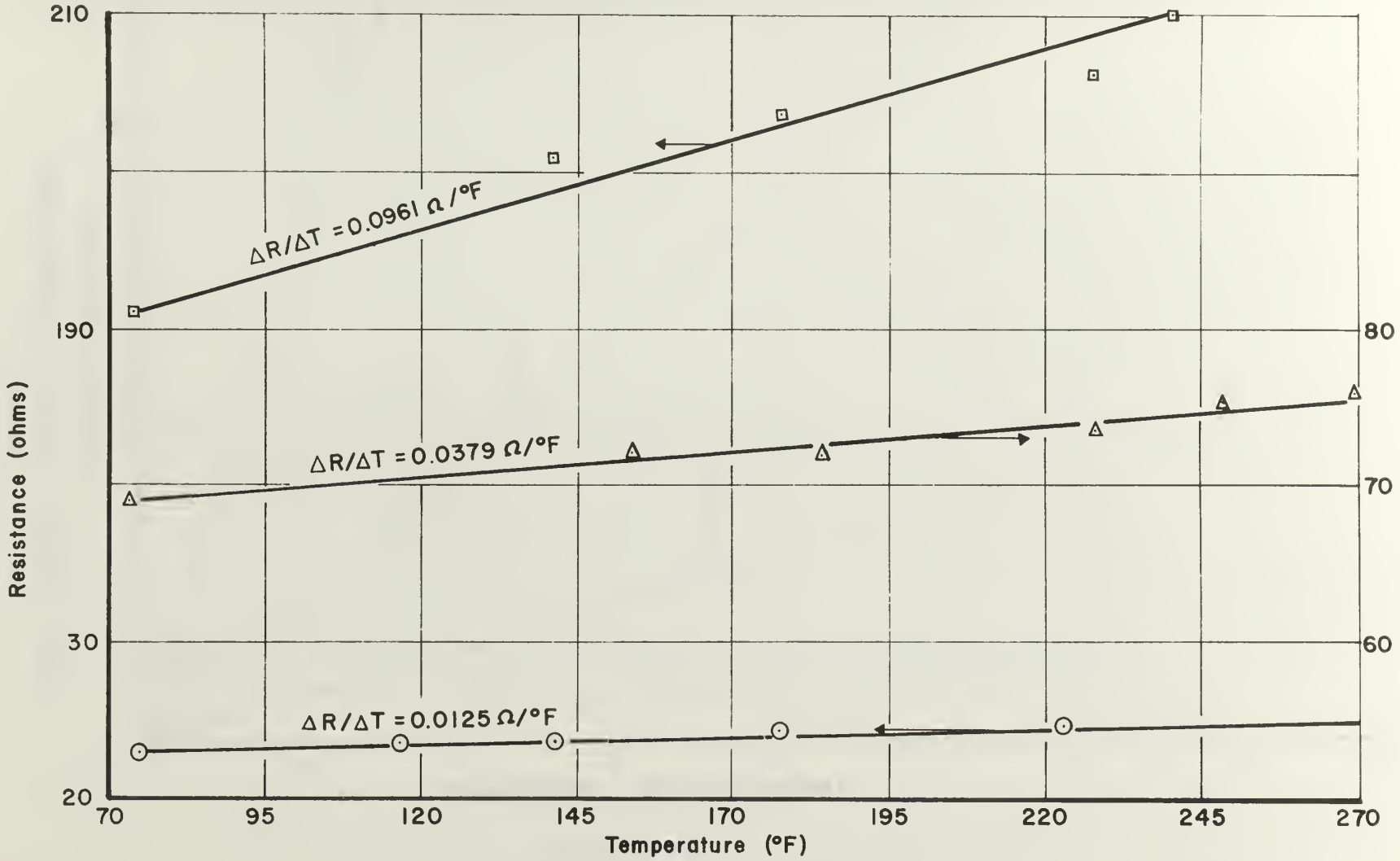

TYPICAL HEAT SENSOR CALIBRATION
FIGURE 12

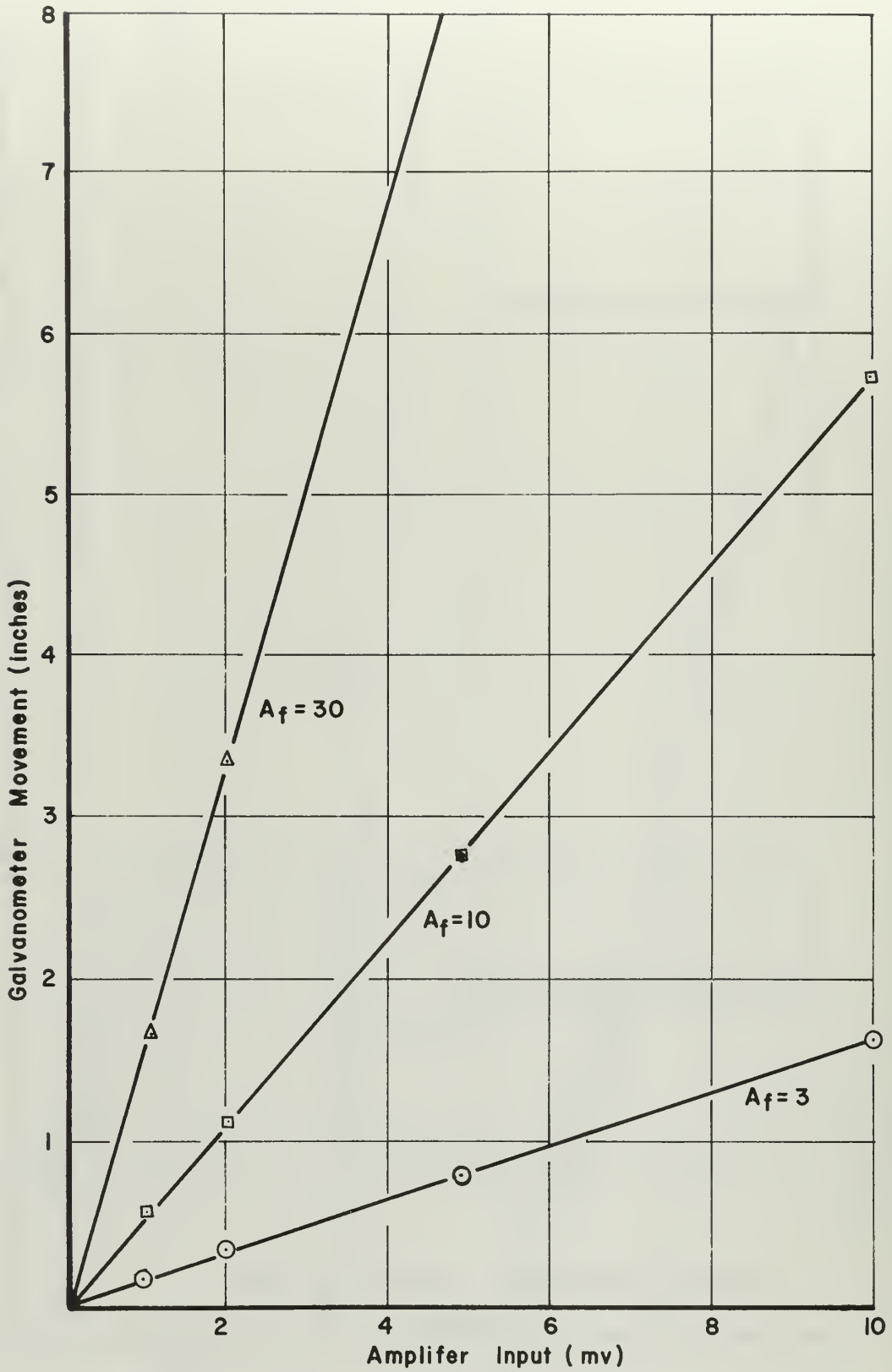

HEAT SENSOR CIRCUIT CALIBRATION
FIGURE 13

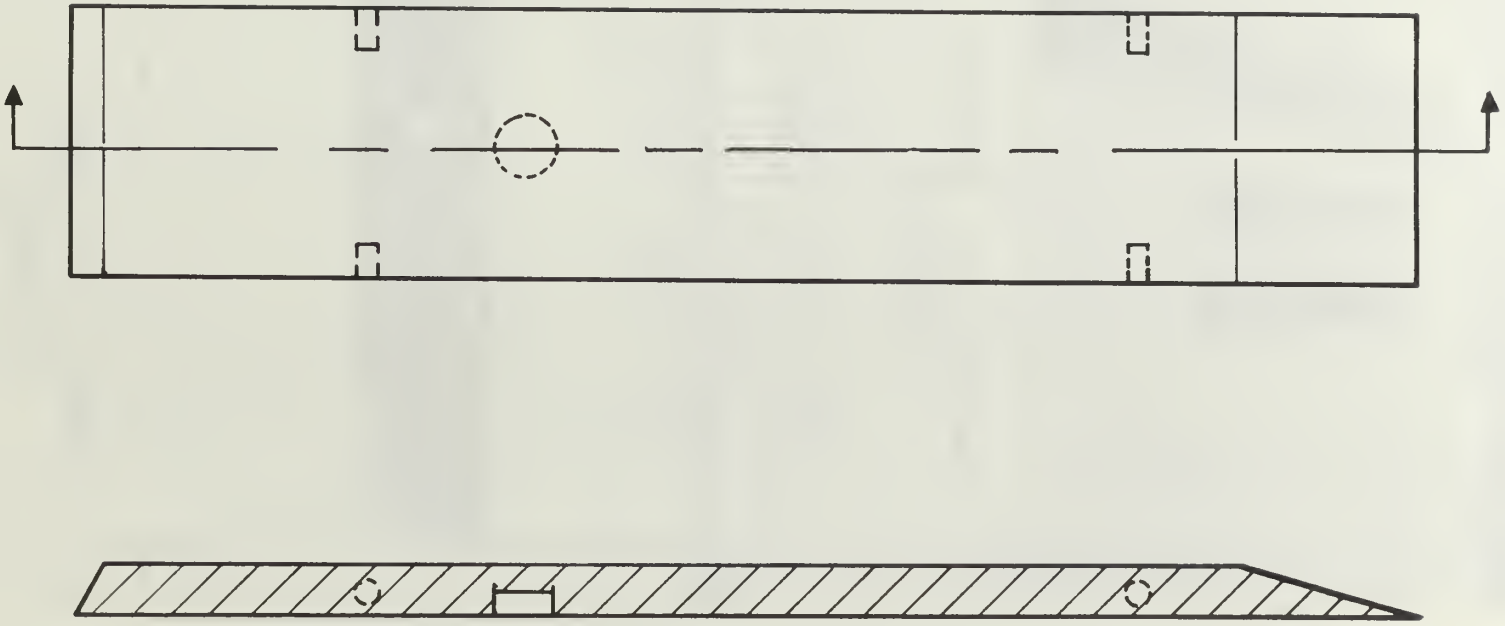

COMPLETED FUEL SLAB

FIGURE 14

DAMAGED HEAT SENSORS
FIGURE 15

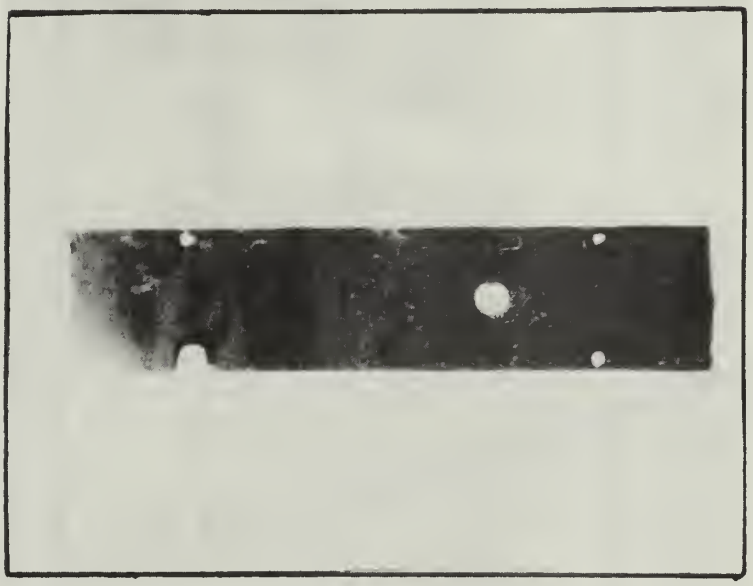

BURNED FUEL SAMPLE
FIGURE 16

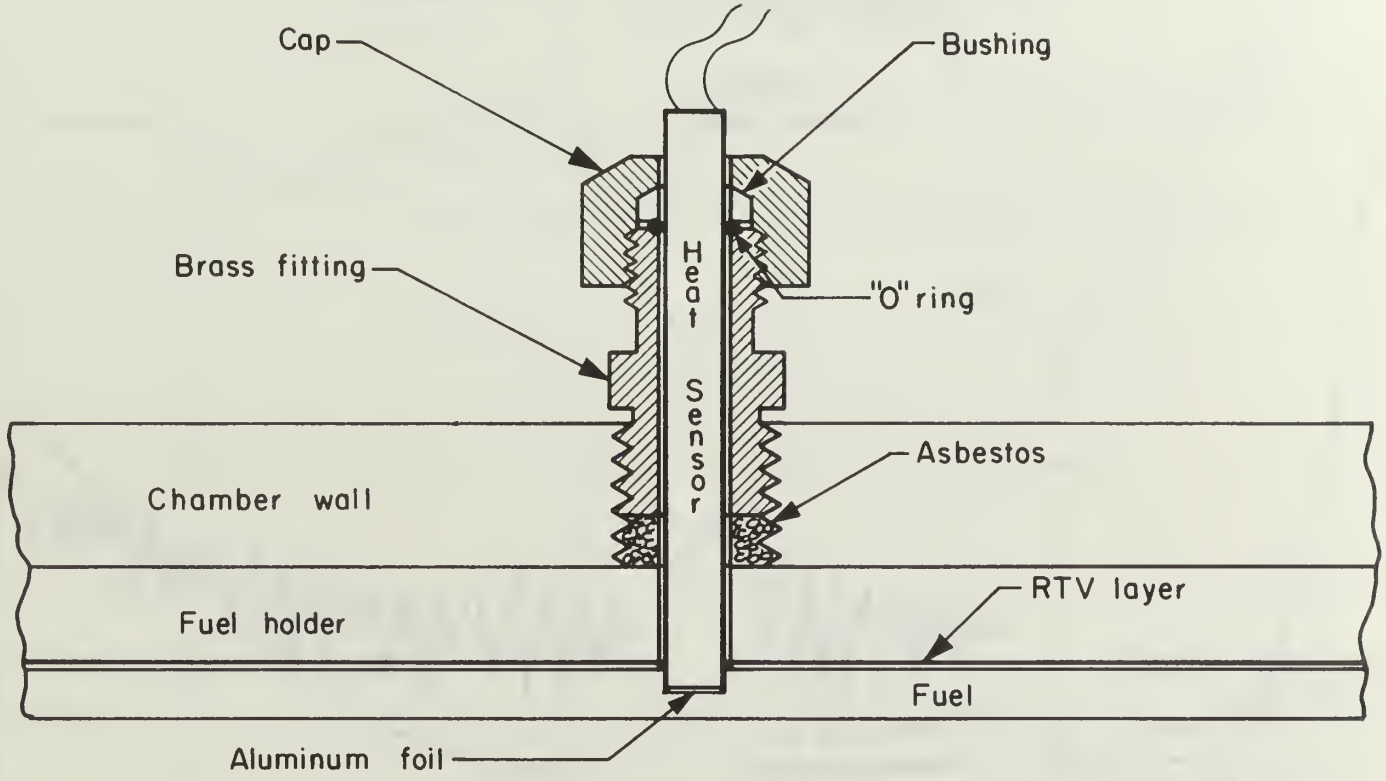

FIGURE 17
CROSS SECTION OF HEAT SENSOR INSTALLATION

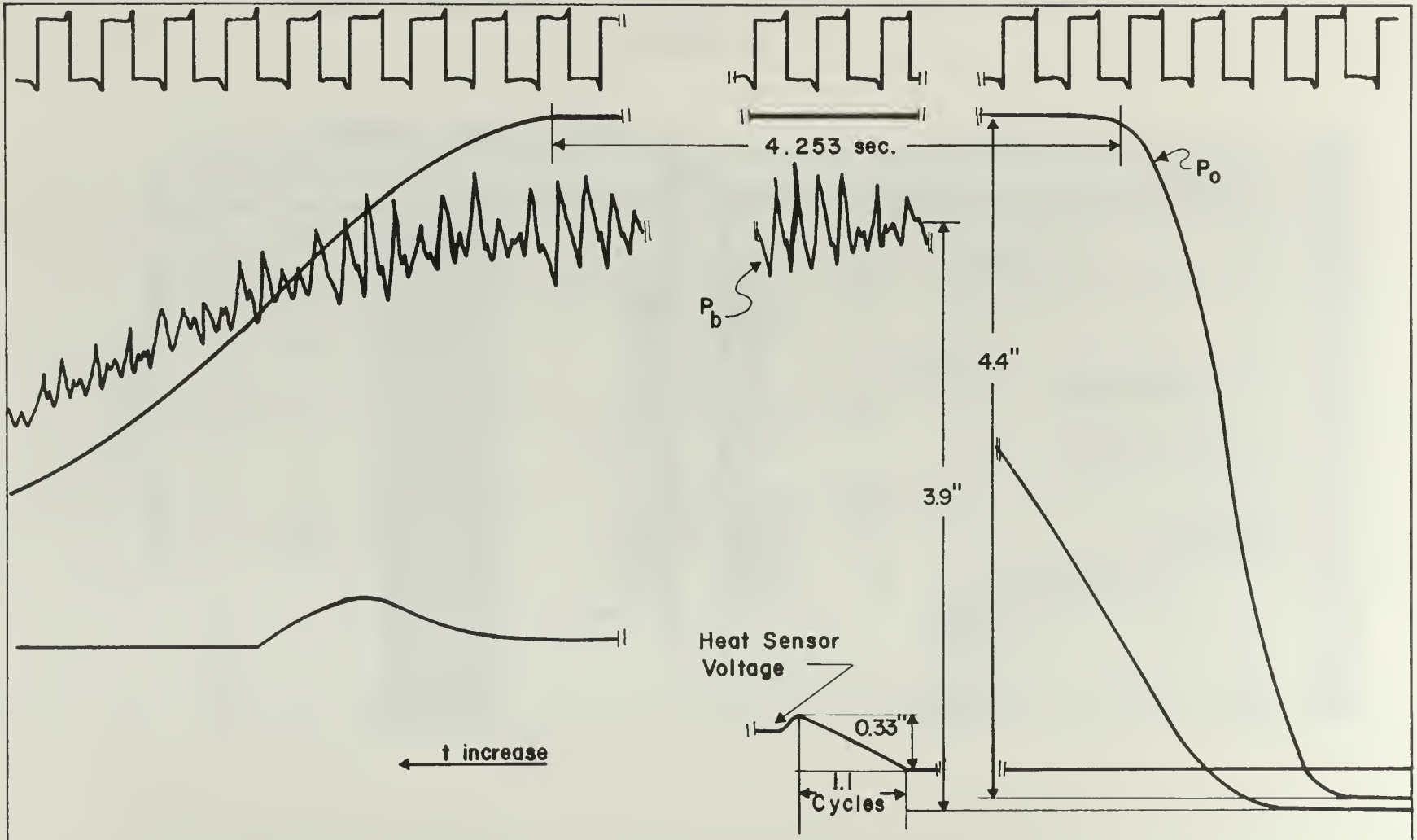

A TYPICAL VISICORDER RECORD

FIGURE 18

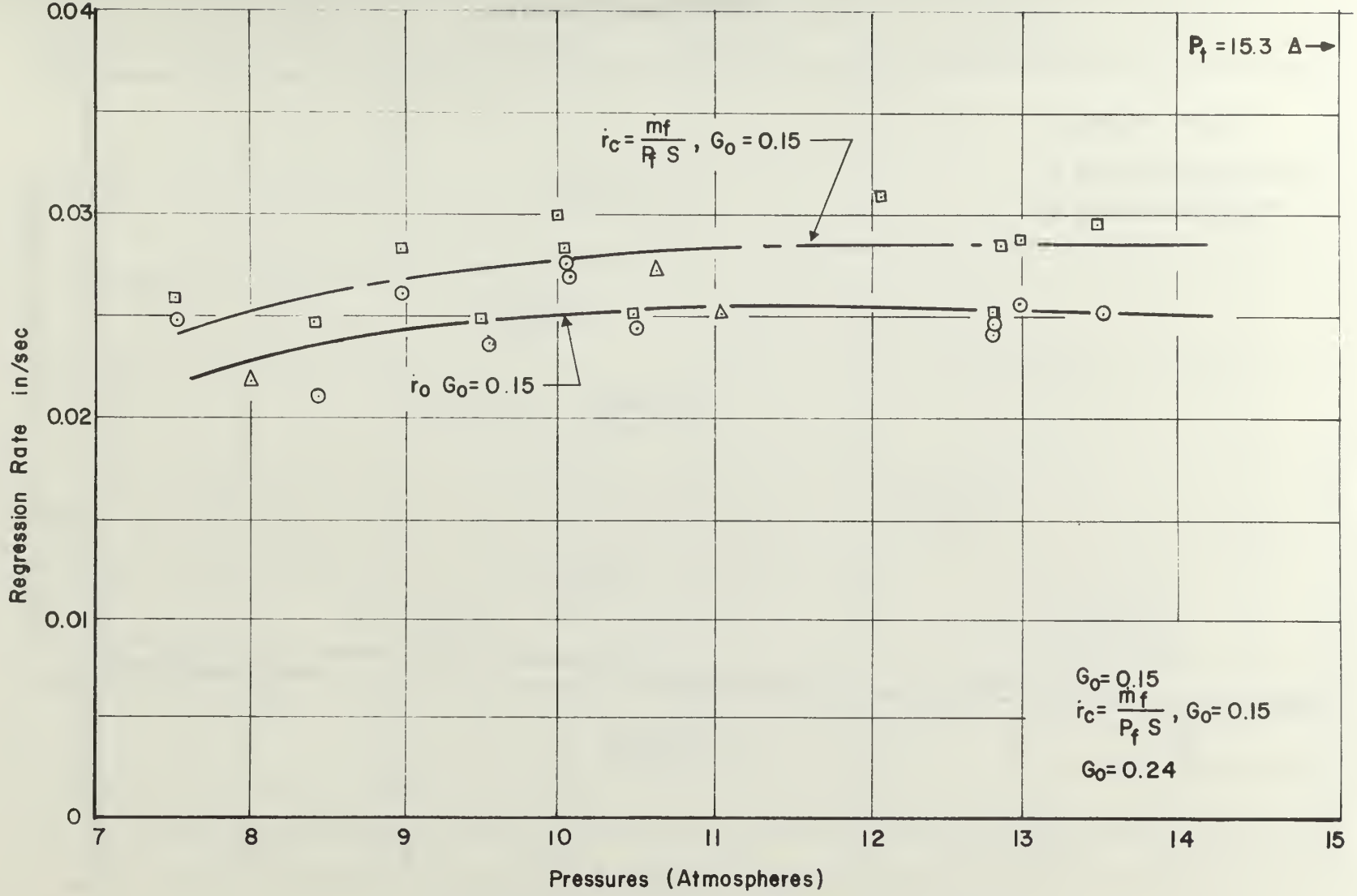

REGRESSION RATE vs CHAMBER PRESSURE
FIGURE 19

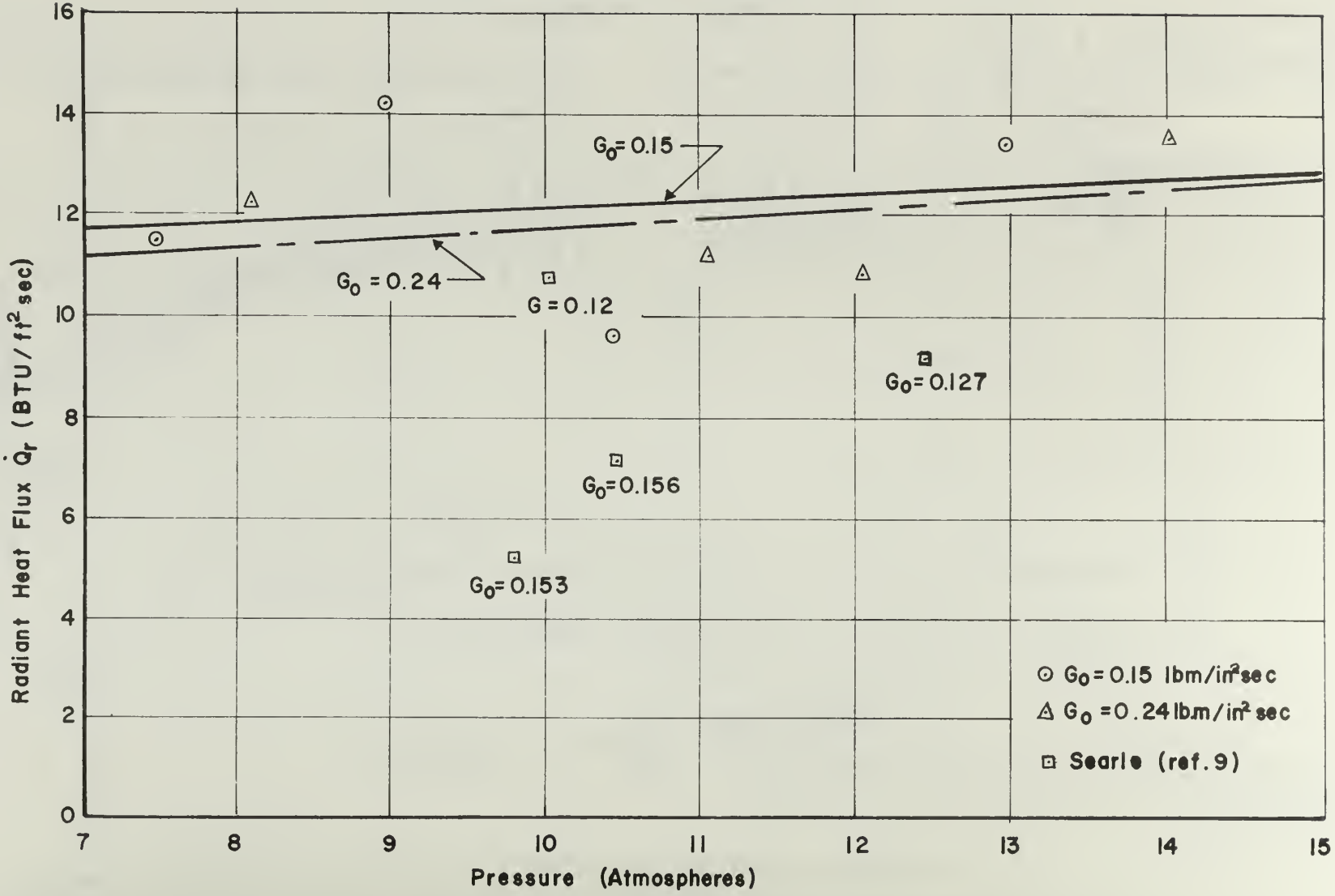

RADIANT ENERGY FLUX vs CHAMBER PRESSURE
FIGURE 20

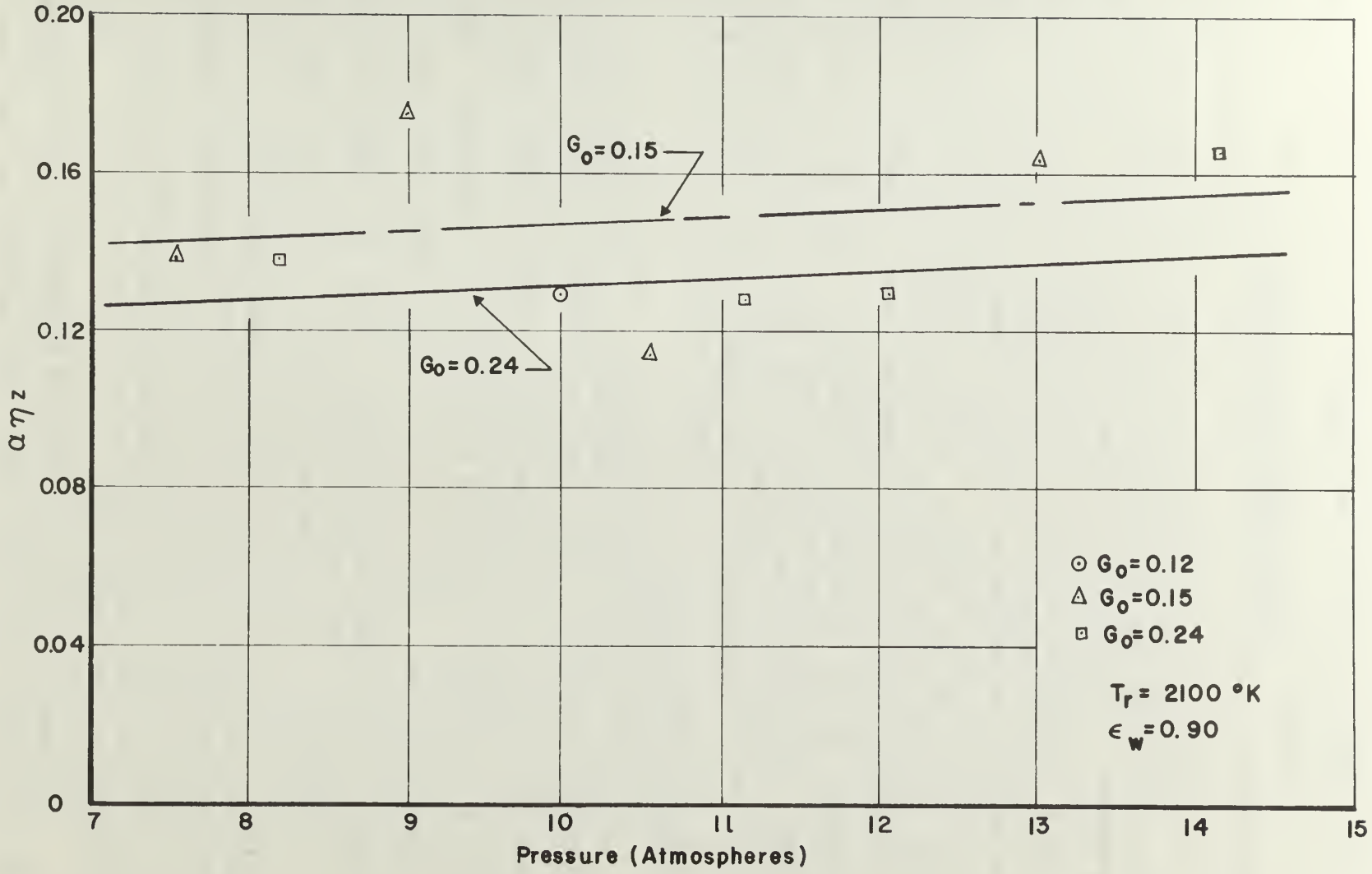

$\alpha \eta z$ vs CHAMBER PRESSURE

FIGURE 21

APPENDIX A

HEAT SENSOR CONSTRUCTION

Although not the primary object of the experimental program, a description of how the sensors were constructed and a discussion of some of the problems encountered would be helpful to anyone who might attempt to construct a similar device in the future. A short summary of the theory of operation of thin-film thermometers was included in the discussion of the experiments conducted. With this theory in mind, and remembering some of the special requirements of the intended application, the sensors were constructed in the following manner.

A minimum substrate thickness of 0.0625 inch was required in order to apply the semi-infinite body heat conduction theory. To provide support for the lead wires, a rod 2 inches in length was selected as a substrate. Each 2 inch piece was taken from a 12 inch length into which a groove 0.0125 inch deep had been cut on the opposite sides of a diameter. The grooves provided a recess for the lead wires. A 0.010 inch by 5 inch diamond saw, mounted in a milling machine, was used to cut the grooves into the rod. One end of each 2 inch length was polished to provide a surface for the metal film.

Although a polish of optical quality is not required for the application of a film, the surface must be free of visible scratches. Thin films will not bridge small

imperfections. Initial attempts to obtain a suitable surface were only partially successful. A small lapping machine was adapted such that four rods could be polished at one time. The difficulty encountered with this approach apparently stemmed from small pieces of the glass remaining suspended in the polishing medium. Approximately 25 per cent of the rods polished, using the lapping machine, retained visible scratches. Better results were obtained by using a vertical sanding wheel covered with a used 600 grit disk. This method successfully removed the imperfections left by the diamond saw when the rods were cut to length. A final polish was obtained by using a felt buffing wheel with rouge as a polishing agent.

After polishing, a thin film of platinum was painted on the gage face and 0.25 inch down each groove. The paint used was Hanovia Liquid Bright Platinum Solution #05X. A sufficiently thin coating was obtained by applying the paint with a #00000 camel hair spotting brush. Following an air drying time, the rods were slowly raised to a temperature of 1200^{o}F and held at that temperature for 15 minutes to insure a positive metal to substrate bond. Films constructed in this manner had resistances which varied between 17 and 200 ohms. The firing cycle took approximately one hour. Thin metal films exhibit unstable resistance characteristics over extended periods of time. To minimize this instability, each film was subjected to two annealing cycles.

During a cycle the film was soaked at 1000°F for four hours followed by a furnace cool to room temperature.

The next step in constructing the heat sensors was to attach the signal leads to the film. Initial attempts to make suitable connections were only partially successful. The first method attempted was to fuse an outer sleeve of pyrex to the 0.225 rod with platinum wires in the grooves prior to applying the film. This process required repolishing the entire assembly before the film could be completed. A good electrical circuit was obtained by first firing a small area of platinum paint around the end of each wire and then applying a complete film. Only one assembly was completed in this manner. Another approach attempted was attaching a 0.010 inch platinum wire to the portion of the film in the groove with silver solder. A sleeve of pyrex was then potted over the leads. Figure 4 shows the sensors which were made in the preceding ways. These methods produced heat sensors which seemed to function correctly. They were abandoned because of the excessive time required to repolish the fused assembly, and several of the soldered sensors lost electrical continuity unexplainably. Satisfactory results were obtained by attaching 0.010 inch copper wires to the film using ECCOBOND solder 58C. This epoxy type material had a maximum use temperature of 530°K. For the intended application no problems were anticipated as the solder was at least 1/16 inch below the fuel surface. At this depth the temperature of the fuel was considerably

below its surface temperature. For the combustion chamber pressures used in the experiments, the surface temperature was of the order of 475 to 700°K.

A thin layer of magnesium floride was evaporated over the sensor face to insulate the metal film from the carbon black coating which was subsequently applied. As was the case with nearly every step of sensor construction, several attempts were made before an effective coating was achieved. The magnesium floride layer must have a thickness of the order of one micron. Standard vacuum deposition techniques were used to apply the coating. If the source of insulating material is considered a point, and a cosine distribution for the density of the vapor is assumed, the mass of material which must be evaporated to obtain a specified thickness can be determined from the following relation.

$$m_{MgF_2} = \tau \pi d \rho_{MgF_2} \qquad \text{(A1)}$$

In Equation A1, τ is the thickness of the coating and d the distance of the specimen from the source of material. If τ is one micron and d equals 10 cm, 10mg of magnesium floride must be evaporated. The effectiveness of the coating seemed to depend on the cleanliness of the surface prior to applying the material. Cleaning the surface with a weak solution of Aqua Regia in water gave the best results.

The carbon black coating was painted over the MgF_2 insulation with a small paint brush. The carbon black

solution applied had an absorbtivity of 0.89 and was manufactured by Thermogage Corporation. After application of the coating, the sensor assembly was heated to 200°F. This procedure was necessary to determine if the coating of MgF_2 was bonded to the metal film sufficiently to expand and contract evenly during heating and cooling cycles. If the coating was not properly bonded, resistance changes of as much as 15,000 ohms were noted. Approximately 10 per cent of the coatings were unsatisfactory.

To facilitate mounting the sensor into the pressurized combustion chamber, the film substrate assembly was incased in a paper phenolic holder. The holders were hollow cylinders 3 inches long. The film-substrate assembly was inserted into the cylinder and potted with APCO #210 high temperature epoxy resin. After allowing the epoxy to cure, the sensor was completed by adding a transparent window. A completed sensor measured 0.31 inches in diameter and 3 inches long. Figure 3 shows the various components of a heat sensor.

APPENDIX B

HEAT SENSOR CIRCUIT ANALYSIS

The thin-film thermometer is a passive instrument which requires an excitation current to operate as a heat sensing device. The assumptions were: The heat sensor excitation current (I_h) was constant, and the bucking voltage resistance did not cause any significant error in the output signal. The Astro Data 885 Differential Amplifier had an input impedance greater than 100 megohms and appeared as an open circuit to the power supply. Referring to Figure 9, and assuming a sensor resistance of 50 ohms, the power supply voltage required to provide an I_h of 0.5ma was computed to be 10.1 volts,

$$\begin{aligned} E_{ps} &= (20{,}160 + 50)\ I_h \\ &= (20{,}210)(0.5) \times 10^{-3} \\ &= 10.1 \text{ volts} \end{aligned}$$

To establish that the excitation current remained constant, the sensor resistance was assumed to increase by 100 ohms. This change was much greater than those which actually occurred during the experiments. For a resistance change of 100 ohms, the change in I_h was less than 1 per cent.

$$\begin{aligned} I_h &= 0.5 \times 10^{-3} - \frac{E_{ps}}{20{,}210 + \Delta R} \\ &= 0.5 \times 10^{-3} - \frac{10.1}{20{,}310} \\ &= 0.0025 \times 10^{-3} \text{ amps} \end{aligned}$$

$$\text{per cent change} = 100 - \frac{I_h + \Delta I_h}{I_h} \times 100$$

$$= -0.5 \text{ per cent}$$

The effect of the resistance of the bucking voltage potentiometer on the heat sensor output signal may be determined by using simple circuit laws. For a sensor resistance of 50 ohms, the steady state voltage drop across the sensor would be 25 milli-volts. The portion of the 50 kilohm resistance required in the signal return circuit to cancel this voltage was 208 ohms.

$$R_{pot} = \frac{25 \times 10^{-3}}{6} \times (50 \times 10^{3})$$

$$= 208 \text{ ohms}$$

The total resistance of the signal return circuit exclusive of the output side of the amplifier was then at least 100 kilohms. Sensor voltage changes during the experiments were no larger than 5 milli-volts. An increase of 10 milli-volts in the sensor signal caused a current flow of 1×10^{-10}a.

$$\frac{\Delta V}{R} \approx I \approx \frac{10 \times 10^{-3}}{100 \times 10^{-6}}$$

$$\approx 1 \times 10^{-10} \text{ amps}$$

The voltage drop occurring in the 208 ohm resistance was then equal to 2.08×10^{-8} volts.

$$V = (1 \times 10^{-10})(208)$$

$$= 2.08 \times 10^{-8} \text{ volts}$$

This value was at least an order of magnitude less than the sensor signal and was neglected.

APPENDIX C

SAMPLE CALCULATIONS

Figure 18 is a tracing of the strip chart record of experiment number 12. The results of this experiment were evaluated below to illustrate the procedure utilized to determine the experimental results from the data recorded during the experiments. The figures referenced in the outline of the procedure refer to the calibration records for the instrumentation used.

Burning time: 85.1 cycles = 4.253 sec.

Fuel sample	Weight	Thickness
Before	33.225 gms	0.214 in.
After	14.424 gms	0.1045 in.
ΔW =	18.801 gms	t = 0.1095 in.

Oxygen Plenum Chamber Pressure (P_o)

4.4 in. = 440 psig (Figure 10)

Combustion Chamber Pressure (P_b)

3.9 in. = 195 psig (Figure 10)

$$P_b = \frac{195}{15} = 13.00 \text{ atm.}$$

Oxygen mass flow for choke diameter of 0.1068 in.

$$\dot{m}_o = 0.101 \text{ lbm/sec (Reference 20)}$$

Oxygen mass flux

$$G_o = \frac{0.101}{0.675} = 0.148 \text{ lbm/in}^2\text{sec}$$

Radiant heat transfer rate ($A_f = 30$)

0.33 in. = 0.2 mv (Figure 13)

$$\Delta T = \frac{0.2 \times 10^{-3}}{0.5 \times 10^{-3} \ (0.01003)} = 39.88^{\circ}F$$

1.1 cycles = 55 msec

$$\dot{Q}_g = \frac{\sqrt{\pi} \ (0.0737)}{2} \left(\frac{39.88}{(5.5)^{\frac{1}{2}} \times 10^{-1}} \right)$$

$$= 11.107 \ BTU/ft^2sec$$

$$\dot{Q}_r = \frac{11.107}{(0.89)(0.93)}$$

$$= 13.419 \ BTU/ft^2sec$$

Burning rates

$$\dot{m}_f = \frac{18.801 \ gms}{4.253 \ sec}$$

$$= 4.421 \ \frac{gms}{sec}$$

$$\dot{r}_f = \frac{0.1095 \ in.}{4.253 \ sec}$$

$$= 0.0257 \ \frac{in.}{sec}$$

$$\dot{r}_c = \frac{4.421 \ \frac{gms}{sec}}{1.066 \ \frac{gms}{cc} \ (9.1) \ in^2 \ \frac{1 \ cc}{6.102 \times 10^{-2} \ in^3}}$$

$$= 0.0278 \ \frac{in.}{sec}$$

DISTRIBUTION LIST

		No. Copies
1.	Defense Documentation Center Cameron Station Alexandria, Virginia 22314	20
2.	Library Naval Postgraduate School Monterey, California 93940	2
3.	Commander, Naval Air Systems Command Navy Department Washington, D. C. 20360	1
4.	Prof. R. E. Reichenbach (Thesis Advisor) Department of Aeronautics Naval Postgraduate School Monterey, California 93940	5
5.	Dr. G. A. Marxman Stanford Research Institute Menlo Park, California 94025	1
6.	Mr. R. J. Muzzy United Technology Center Sunnyvale, California 94086	1
7.	Major H. L. Searle, USMC 5513 Yorkshire Street Springfield, Virginia 22151	1
8.	Mr. B. Drimmer (Code 0331) Naval Ordnance Systems Command Washington, D. C. 20360	1
9.	Dr. E. Lamar, Chief Scientist Naval Air Systems Command Washington, D. C. 20360	1
10.	Major John MacCallum Advanced Research Projects Agency 1111 19th Street Arlington, Virginia 22209	1
11.	Dr. F. T. Byrne Office of Naval Research Navy Department Washington, D. C. 20390	1

DISTRIBUTION LIST (CONT'D)

		No. Copies
12.	Chairman, Department of Aeronautics Naval Postgraduate School, Monterey, California	1
13.	Professor A. E. Fuhs, Department of Aeronautics Naval Postgraduate School, Monterey, California	1
14.	LT Carl E. Bruntlett, USN Attack Squadron ONE TWO FIVE NAS Lemoore, California 93246	3

DOCUMENT CONTROL DATA - R&D

(Security classification of title, body of abstract and indexing annotation must be entered when the overall report is classified)

1. ORIGINATING ACTIVITY *(Corporate author)*
Naval Postgraduate School
Monterey, California

2a. REPORT SECURITY CLASSIFICATION
UNCLASSIFIED

2b. GROUP

3. REPORT TITLE

A PARAMETRIC STUDY OF THE RADIANT ENERGY FLUX TO THE FUEL SURFACE DURING HYBRID COMBUSTION

4. DESCRIPTIVE NOTES *(Type of report and inclusive dates)*
Thesis.

5. AUTHOR(S) *(Last name, first name, initial)*
Bruntlett, Carl E.
LT USN

6. REPORT DATE	7a. TOTAL NO. OF PAGES	7b. NO. OF REFS
December 1967	80	22

8a. CONTRACT OR GRANT NO.	9a. ORIGINATOR'S REPORT NUMBER(S)
b. PROJECT NO.	
c.	9b. OTHER REPORT NO(S) *(Any other numbers that may be assigned this report)*
d.	

10. AVAILABILITY/LIMITATION NOTICES
[redacted]

11. SUPPLEMENTARY NOTES	12. SPONSORING MILITARY ACTIVITY
	NAVAL AIR SYSTEMS COMMAND

13. ABSTRACT

The heat transfer rate to the solid fuel surface during hybrid combustion has been considered as the primary rate limiting phenomenon in one theoretical analysis of the hybrid combustion process. One mode of heat transfer involved is the radiant energy flux to the fuel surface. Little data are available for direct measurement of this portion of the heat transfer. Experiments were conducted in which the radiant flux to the fuel surface was measured by utilizing thin-film thermometers as a heat sensing device. A limited amount of data was obtained for the radiant flux during combustion of the polystyrene-oxygen system. These data established a range of values for the radiant flux of 10-14 BTU/ft^{2}sec. Combustion chamber pressure was varied between 7 and 14 atmospheres. Values of oxidizer mass flux, 0.15 and 0.24 lbm/in^2 sec, were used to obtain the data. The results appeared to verify the analytical formulation for fuel linear regression rate in terms of the physical coupling between the convective and radiative heat transfer rates to the fuel surface.

DD FORM 1 JAN 64 1473

14 KEY WORDS	LINK A		LINK B		LINK C	
	ROLE	WT	ROLE	WT	ROLE	WT
Parametric						
Study						
Radiant						
Energy						
Flux						
Hybrid						
Combustion